Global Biogeochemical Cycles

RESEARCH ARTICLE
10.1029/2019GB006305

Key Points:
- Production and export of surface small-particle POC to the OMZ interior coincided with changes in wind stress and precipitation
- A permanent layer of small particles in the upper layer of the OMZ might have a key role in attenuating POC fluxes
- Attenuation rates of small-particle fluxes were equivalent or significantly higher inside the OMZ relative to the well-oxygenated regions

Supporting Information:
- Supporting Information S1

Correspondence to:
R. Rasse,
rjrasse@gmail.com;
rafael.rasse@obs-vlfr.fr

Citation:
Rasse, R., & Dall'Olmo, G. (2019). Do Oceanic Hypoxic Regions Act as Barriers for Sinking Particles? A Case Study in the Eastern Tropical North Atlantic. *Global Biogeochemical Cycles*, *33*. https://doi.org/10.1029/2019GB006305

Received 3 JUN 2019
Accepted 6 NOV 2019
Accepted article online 5 DEC 2019

Do Oceanic Hypoxic Regions Act as Barriers for Sinking Particles? A Case Study in the Eastern Tropical North Atlantic

Rafael Rasse[1,2,3] and Giorgio Dall'Olmo[3,4]

[1]Sorbonne Universités, UPMC Université Paris 06, CNRS, Laboratoire d'Océanographie de Villefranche (LOV) UMR7093, Observatoire Océanologique, Villefranche-sur-Mer, France, [2]Centro de Ciencias Atmosféricas y Biogeoquímica, Instituto Venezolano de Investigaciones Científicas, Caracas, Venezuela, [3]Plymouth Marine Laboratory, Plymouth, UK, [4]National Centre for Earth Observation, Plymouth Marine Laboratory, Plymouth, UK

Abstract In oxygen minimum zones (OMZs), the attenuation rates of particulate organic carbon (POC) fluxes of large particles are known to be reduced, thus increasing the efficiency with which the biological carbon pump (BCP) transfers carbon to the abyss. The BCP efficiency is expected to further increase if OMZs expand. However, little is known about how the POC fluxes of small particles—a significant component of the BCP—are attenuated inside OMZs. In this study, data collected by two BGC-Argo floats deployed in the hypoxic OMZ of the eastern tropical North Atlantic were used to estimate net instantaneous fluxes of POC via small particle during 3 years. This information was analyzed together with meteorological data and published POC fluxes of large particles and allowed us to conclude that (1) major pulses of surface-derived small particles toward the OMZ interior coincided with seasonal changes in wind stress and precipitation; (2) a permanent layer of small particles, presumably linked to microbial communities, was found in the upper section of the OMZ which might play a key role attenuating POC fluxes; and (3) fluxes of large particles were attenuated less efficiently inside this poorly oxygenated region than above it, while attenuation of small-particle fluxes were equivalent or significantly higher inside the OMZ. These results highlight that more information about the processes controlling the fluxes of small and large particles in hypoxic OMZs is needed to better understand the impact of hypoxic OMZs on the BCP efficiency.

1. Introduction

The biological carbon pump (BCP) is a set of mechanisms that removes atmospheric carbon dioxide by exporting particulate organic carbon (POC) from the upper ocean toward its interior (Volk & Hoffert, 1985). As it sinks to the abyss, most POC is remineralized by bacteria back to CO_2 and reexchanged with the atmosphere on time scales that depend on the depth at which remineralization takes place (Kwon et al., 2009). Thus, understanding what controls POC fluxes and their remineralization is crucial to mechanistically predict how the BCP controls atmospheric CO_2 concentration and in turn mitigates the Earth's climate (Falkowski et al., 1998; Parekh et al., 2006; Sarmiento & Gruber, 2006).

Ocean regions with a key role in POC remineralization are oxygen minimum zones (OMZs). OMZs are water masses with low oxygen levels located at intermediate depths, which represent ~5% of the oceans volume (e.g., 200–1000 m, $O_2 < 60$ μmol kg^{-1}, Deutsch et al., 2011; Paulmier & Ruiz-Pino, 2009). These regions appear to reduce POC remineralization rates allowing POC to reach deeper waters relative to oxygenated areas ($O_2 > 120$ μmol kg^{-1}, Cavan et al., 2017, Devol & Hartnett, 2001; Engel et al., 2017; Martin et al., 1987; Roullier et al., 2014; Van Mooy et al., 2002). Thus, the hypothesis that the potential expansion of OMZs could increase the efficiency of the oceanic BCP is strengthening (e.g., Cavan et al., 2017; Deutsch et al., 2014; Engel et al., 2017; Le Moigne et al., 2017; Oschlies et al., 2019; Schmidtko et al., 2017; Stramma et al., 2008). However, this hypothesis is based on measurements of the attenuation rates of POC fluxes mostly due to large sinking particles because these are the predominant fraction of particles collected by conventional sediment traps (e.g., >100 μm; Arístegui et al., 2009; Buesseler et al., 2007; Devol & Hartnett, 2001; Engel et al., 2017; Gardner et al., 1985; Martin et al., 1987; Trull et al., 2008; Van Mooy et al., 2002).

Small particles with sizes <100 μm can also transport significant amounts of POC to the abyss. Although these particles can be formed both in the sunlit and mesopelagic regions by photo- and chemosynthesis (Close et al., 2013; Herndl et al., 2005; Raven, 2009; Reinthaler et al., 2006; Roullier et al., 2014; Thunell

et al., 2000; Wright et al., 2012), physical and biological fragmentation of large sinking particles is thought to be one of the main sources of small particles in the mesopelagic region. Ultimately, fragmentation contributes to small-particle POC fluxes toward the abyss (e.g., >200 m depth, Boyd et al., 2019; Burd & Jackson, 2009; Dilling & Alldredge, 2000; Giering et al., 2014; Jumars et al., 1989; Lampitt et al., 1990; Mayor et al., 2014; Stemmann et al., 2004).

In the North Atlantic, fragmentation-derived small-particle fluxes contribute between 40% and 85% of the total POC fluxes in the first 650 m depth, and these fluxes can show a strong seasonality linked to changes in the mixed layer depth (MLD) (Dall'Olmo & Mork, 2014; Durkin et al., 2015; Giering et al., 2016). These results demonstrate that the export of these tiny particles is a significant component of the BCP that varies over time. Little is known however about POC fluxes via small particles and their attenuation rates in OMZs.

POC fluxes measured by conventional sediment traps are mostly due to large sinking particles because small particles are not efficiently captured by these tools (Arístegui et al., 2009; Buesseler et al., 2007; Gardner et al., 1985; Trull et al., 2008). Although methods exist to collect small particles (e.g., Marine Snow Catcher, Durkin et al., 2015; Giering et al., 2016; Riley et al., 2012), these are still labor intensive and time consuming and provide data with limited temporal, vertical, and spatial resolution. Therefore, complementary techniques are needed to assess what drives the temporal variations and attenuation rates of POC fluxes by small particles in OMZs.

Net instantaneous fluxes of POC by small particles can be estimated from quasi-continuous measurements of particle backscattering (b_{bp}, a proxy of POC; Stramski et al., 1999, 2004) collected by autonomous profiling floats (i.e., "BGC-Argo," Dall'Olmo & Mork, 2014). Even though a typical range of 0.2–20 μm is assumed for these small particles (Dall'Olmo & Mork, 2014), recent findings have demonstrated that the small particles detected by b_{bp} should range approximately between ~1 and 10 μm at least in the sunlit oligotrophic ocean (Organelli et al., 2018). Thus, the dynamics of these small particles can be investigated using data from BGC-Argo floats to fill knowledge gaps about the BCP (e.g., Bishop & Wood, 2009; Dall'Olmo et al., 2016; Estapa et al., 2017, 2019; Lacour et al., 2017; Mignot et al., 2018). However, so far BGC-Argo observations have not been used to study particle dynamics inside OMZs.

One important OMZ is located in the eastern tropical North Atlantic (ETNA). The ETNA OMZ is a hypoxic region (e.g., O_2 < 60–120 μmol kg^{-1}) that has been expanding significantly over the last decades (Stramma et al., 2008). Hypoxic regions are important because they occupy an oceanic volume ~100-fold higher than anoxic areas (Engel et al., 2017; Paulmier & Ruiz-Pino, 2009; Stramma et al., 2010).

The aim of this study was to investigate particle export fluxes and their attenuation rates in the hypoxic OMZ of the ETNA. We used data collected from two BGC-Argo floats deployed in the ETNA OMZ to estimate vertically resolved net instantaneous fluxes of POC by small particles during 3 years. This information, together with complementary meteorological data retrieved from remote sensing and published POC fluxes by large particles, allowed us to demonstrate that (1) major pulses of small particles derived from the fragmentation of large aggregates were related to seasonal changes in wind stress and precipitation; (2) a permanent layer rich in small particles, presumably linked to bacteria, was present between the upper and intermediate layers of the OMZ and might have a key role attenuating the fluxes of small-particle POC; (3) in the poorly oxygenated waters studied, the attenuation rates of small-particle POC fluxes were equivalent or significantly higher relative to those in the well-oxygenated regions above the OMZ, whereas large particles fluxes were attenuated less efficiently inside the OMZ than above it.

1.1. Site Description

In the ETNA, the seasonal meridional migration of the intertropical convergence zone (ITCZ, Figure 1) drives wind stress and precipitations (Nobre & Shukla, 1996). This forcing contributes to controlling primary production and the export of particles from the surface to the abyss (Pastor et al., 2013; Schlosser et al., 2014; Signorini et al., 1999).

1.2. Methods

1.2.1. External Forcing

Daily area-averaged wind stress (τ, N m^{-2}) was estimated from the Blended Mean Wind Field global data product (http://marine.copernicus.eu/) at all locations of the BGC-Argo profiles (e.g., location: latitude

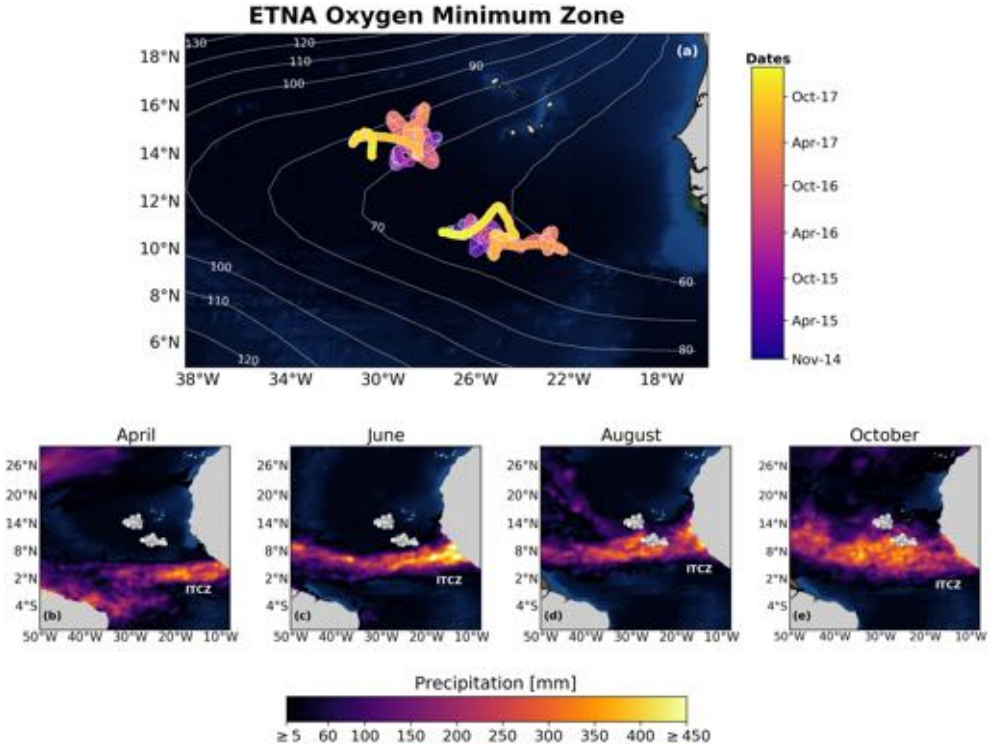

Figure 1. (a) Location of BGC-Argo floats 6901174 (colored upper circles) and 6901175 (colored bottom circles) in the ETNA oxygen minimum zone. White contours are the annual climatology of dissolved oxygen concentration at 400 m depth provided by the World Ocean Data Center (https://www.nodc.noaa.gov/OC5/indprod.html). (b), (c), (d), and (e) are monthly precipitations for April, June, August, and October of 2016, respectively (data source: https://giovanni.gsfc.nasa.gov/giovanni/). These bottom figures highlight the monthly location of the intertropical convergence zone (ITCZ, longitudinal band with high precipitation) with respect to the BGC-Argo floats (white circles).

±0.5° and longitude ±0.5°) for a backward period of 5 days. This backward period started from the day of the profile and ended 5 days before it. These wind products were generated by the European Centre for Medium-Range Weather Forecasts by using scatterometers Advanced scatterometer (ASAT) and Oceansat-2 scatterometer (OSCAT) retrievals with a horizontal resolution of 0.25 × 0.25 degrees.

Similarly, cumulative daily area-averaged precipitation rates (mm d^{-1}) were also extracted at the profile locations and for the 5 days before each profile. These data were retrieved from the TRMM multisatellite precipitation analysis with a temporal and spatial resolution of 3 hours (3B42RT) and 0.25 × 0.25 degrees, respectively (https://giovanni.gsfc.nasa.gov/giovanni/).

1.2.2. Bio-optical and Physicochemical Parameters

To assess how the ITCZ migration drives particle dynamics in this region, we used data collected with high temporal and vertical resolution by two Biogeochemical-Argo (BGC-Argo) floats. These floats are uniquely identified by World Meteorological Organization (WMO) numbers 6901174 and 6901175 and profiled every 5 days in the first 1000 m depth of the ETNA OMZ since November 2014 until January 2018 (n = 235–245 upward profiles for each BGC-Argo float, Figure 1). The two floats remained within a relative small area that ranged between 310×390 and 250×690 km^2, respectively, and were separated by a meridional distance of approximately 600 km (Figure 1). This separation allowed us to assess how the seasonal location of the ITCZ (e.g., Figure 1) impacted surface stratification and related production and export of particles in two regions of the ETNA OMZ.

BGC-Argo floats were equipped with a CTD, Aanderaa oxygen optode, and WETLabs sensors to measure upward profiles of temperature (T), conductivity, depth, dissolved oxygen (O_2), chlorophyll fluorescence (*chl*), and total optical backscattering (particles + pure seawater) at 700 nm. Raw data of total backscattering and fluorescence were converted into particle backscattering (b_{bp}) and *chl* following standard protocols (Schmechtig et al., 2014, 2015). In addition, b_{bp} and *chl* spikes were removed by applying

a median filter with a window size of three data points (e.g., Briggs et al., 2011; Dall'Olmo & Mork, 2014).

1.2.3. Minimizing Uncertainties in b_{bp} Estimates

Biases in raw b_{bp} due to instrumental drift were first removed (see supporting information). Furthermore, an additional potential problem was identified in the b_{bp} data from one of the floats. For the first 14 months of operation, the b_{bp} meters of both floats were programmed to collect measurements with a vertical resolution of 10 dbars below 600 meters depths (close to isopycnal 27.2 kg m^{-3}). Subsequently, the b_{bp} meter resolution was increased to 1 dbar (supporting information). For float 6901175, this change in the vertical resolution of b_{bp} measurements did not affect the mean b_{bp} values determined in the water masses below 600 meters depth (supporting information). In contrast, for float 6901174, during the last 4 months (August 2015 and January 2016) of the sampling period with low vertical resolution, the mean b_{bp} were ~20% lower in the same deepwater masses than after the change in resolution (supporting information). The reason for this change is unclear but could be similar to the problem described for these sensors by Wojtasiewicz et al. (2018). These authors hypothesized that this decrease in b_{bp} likely could have resulted from (1) a longer time response of the sensor to achieve optimal performance and/or (2) variations in the light source intensity due to changes in the water temperature (Sullivan et al., 2013; Wojtasiewicz, Trull, et al., 2018). Thus, the b_{bp} data collected during this period were not used to calculate the stocks of POC. The latter data were only exploited to describe the small-particle dynamics above 600 m depth (0.2–20 μm, e.g., sections 2.2 and 2.3 and Figures 4–6) because above this depth, there were no changes in the vertical resolution of b_{bp} measurements.

1.2.4. Delimiting MLD, Productive Region, and OMZ

Potential density (σ_θ) was derived from T and S (salinity) and the MLD was computed using a σ_θ threshold difference of 0.03 kg m^{-3} from a depth of 1 meter (de Boyer Montégut et al., 2004). To derive a proxy for stratification, we calculated the difference between σ_θ at 100 m and 10 m depth (σ_θ, e.g., Lozier et al., 2011). This proxy allowed us to synthesize in a single metrics the effects that wind stress and precipitation had on surface stratification to investigate the related production of surface particles (e.g., Figures 2 and 3). The bottom of the productive region (z_p) was estimated as the depth at which *chl* decreases below 0.05 mg m^{-3} (Figures 2 and 3). We used *chl* to define the productive layer where living phytoplankton are present because our technique to compute export requires that no production is taking place below a given layer of the water column. We found that z_p was always deeper than the MLD with average values (±standard deviation, WMO number) of 139 m (±12, 6901174) and 130 m (±13, 6901175); z_p approximately followed the 26.6 kg m^{-3} isopycnal (Figures 2 and 3).

Dissolved oxygen (O_2) concentrations were quality controlled following published procedures (supporting information, Takeshita et al., 2013). No well-defined method to delimit hypoxic OMZs exists because of the wide range of O_2 concentrations encompassed by them (e.g., <60–120 μM, Stramma et al., 2008). Here, to define the top, center, and bottom of the OMZ, isopycnals were used because they allowed us to consistently delimit, in both sampled regions, the water mass characterized by hypoxic conditions (oxygen concentrations <60–90 μM). To this end, the isopycnal corresponding to the local minimum of dissolved oxygen concentration was used as the reference isopycnal for the center of the OMZ core. For the whole time series, we found that the minimum O_2 concentration (although different in magnitude) occurred approximately along the same central isopycnal (σ_θ = 27.05 kg m^{-3}) in the two regions sampled by the two floats.

After having identified the isopycnal 27.05 kg m^{-3} as the one corresponding to the minimum oxygen concentration along the vertical profile, we selected two additional isopycnals above and below the central isopycnal to define the water mass that contained the OMZ core. These two additional isopycnal were manually selected and differed by ±0.15 kg m^{-3} from the central isopycnal. Although subjective, this choice allowed us to consistently define the water mass that contained the hypoxic region (O_2 < 60–90 μM). Thus, the top (OMZ_{top}), center (OMZ_{center}), and bottom (OMZ_{bottom}) of the OMZ were defined as the isopycnals 26.9, 27.05, and 27.2 kg m^{-3}, respectively (Figures 2, 3, and section 2.1). Although subjective, our choice allows us to define the OMZ core consistently with the subdivision of the water column (by isopycnals) that we adopted to compute POC fluxes (section 1.2.5).

1.2.5. POC Stocks and Export

No published relationships between b_{bp} and POC were available for the mesopelagic ETNA OMZ; thus b_{bp} was converted into POC concentrations (POC, mg m^{-3}) by using a published bio-optical POC-b_{bp}

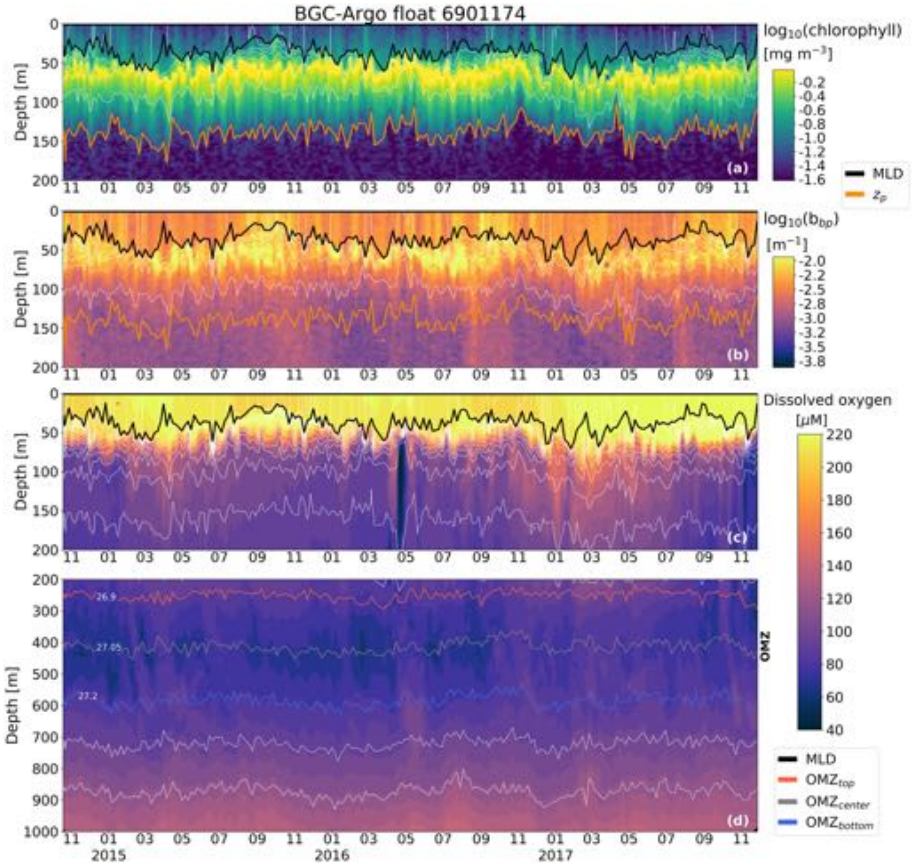

Figure 2. (a) Chlorophyll-a concentration and (b) $\log_{10}(b_{bp})$ in the first 200 m depth for BGC-Argo float 6901174. Orange lines in (a) and (b) are the location of z_p which on average followed the 26.6 kg m^{-3} isopycnal. (c) and (d) present dissolved oxygen concentration in the first 200 m depth and between 200 and 1000 m depth, respectively. Red, gray, and blue lines in (d) indicate the location of OMZ_{top} (σ_Θ = 26.9 kg m^{-3}), OMZ_{center} (σ_Θ = 27.05 kg m^{-3}), and OMZ_{bottom} (σ_Θ = 27.2 kg m^{-3}), correspondingly. Black lines in (a), (b), and (c) are the MLD.

relationship for the surface Atlantic ($\log_{10}$(POC) = 0.870*$\log_{10}(b_{bp})$ + 4.28; Rasse et al., 2017). Predicted POC concentrations (8–26 mg m^{-3}) were similar to those previously measured in the mesopelagic region (≥150–900 m) of the ETNA OMZ (18–60 mg m^{-3}, Martiny et al., 2014).

Water column layers were then delimited using isopycnals separated by a potential density (σ_Θ) threshold of 0.05 kg m^{-3} (e.g., between isopycnals 26.6 and 26.65 kg m^{-3}). The thickness of each layer was calculated as the mean distance separating the two isopycnals during the time series.

Stocks of POC (mg m^{-2}) in progressively deeper layers of the water column were estimated by multiplying the mean thickness of the layers (m) by their corresponding average concentration of POC (mg m^{-3}) for each profile. Specifically, the stocks of POC were computed for the layers delimited from selected isopycnals ($\sigma_{\theta i}$) to the deepest isopycnal sampled by the float (27.5 kg m^{-3}, σ_{max}). We indicate these POC stocks with the notation $iPOC^{27.5}_{\sigma_{\theta i}}$, where $\sigma_{\theta i}$ = 26.6 kg m^{-3} + n, n = 0, 0.05, 0.1, … , 0.8 kg m^{-3}; and 27.5 kg m^{-3} is the deepest isopycnal sampled (e.g., Figures 4 and 5). In addition, to track the temporal variations in surface production of small particles, surface POC stocks were calculated between 1 m and z_p.

Net instantaneous fluxes of POC just below a given isopycnal ($\sigma_{\theta i}$) were computed as the time rate of change of $iPOC^{27.5}_{\sigma_{\theta i}}$ ($E_{\sigma_{\theta i}} = \partial iPOC^{27.5}_{\sigma_{\theta i}}/\partial t$) after applying a pseudo-Gaussian smoothing filter to $iPOC^{27.5}_{\sigma_{\theta i}}$ (e.g., orange and red lines in Figures 7 and 8). Here the main assumptions are a negligible export of particles below σ_{max} and spatial homogeneity of the particle field (Dall'Olmo & Mork, 2014). Thus, positive $E_{\sigma_{\theta i}}$ values correspond to the net rate at which small particles accumulated below a given isopycnal. Uncertainties and details of the method applied to predict POC fluxes are discussed in Dall'Olmo and Mork (2014).

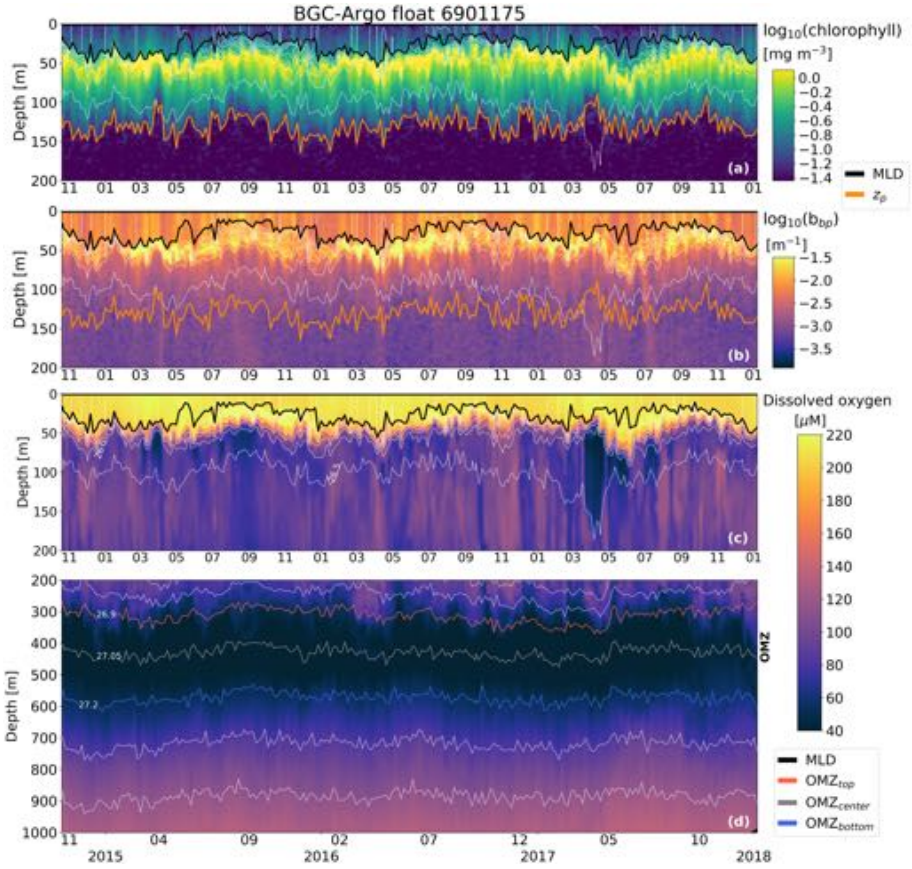

Figure 3. As Figure 2 but for the region sampled by BGC-Argo float 6901175.

Transfer efficiencies (T_{eff}, %) of POC fluxes below z_p and OMZ_{top} were calculated as the ratio between $E\sigma_{oi}$:E_{ref} multiplied by 100 (Buesseler & Boyd, 2009). E_{ref} indicates the POC fluxes just beneath z_p or OMZ_{top}, while $E\sigma_{oi}$ indicates fluxes at progressively deeper isopycnals below z_p or OMZ_{top}.

To compare T_{eff} values in poorly and well-oxygenated water layers that differed in thickness, a new metric denominated "depth-specific attenuation rate" was developed (ΔT, % m^{-1}). This new metric allows one to compare the attenuation of POC fluxes between water layers, independently of the thickness of these layers.

More specifically, ΔT was calculated as: $\Delta T = (T_{eff\text{-}R} - T_{eff\text{-}\sigma})/d^*100$. Here $T_{eff\text{-}R}$ and $T_{eff\text{-}\sigma}$ are the transfer efficiencies at the reference and progressively deeper isopycnals, respectively (e.g., $T_{eff\text{-}\sigma} = E\sigma_{oi}{:}E_{ref}$); d is the distance between the reference and deeper isopycnals.

For water layers above the OMZ (ΔT_{above}), the isopycnal following the depth of the productive region was used as reference and $T_{eff\text{-}\sigma}$ was calculated between isopycnals >26.6 and ≤ 26.9 kg m^{-3} (e.g., Figures 9, 10). Similarly, inside the OMZ layers (ΔT_{inside}), the isopycnal at the top of the OMZ was used as reference and $T_{eff\text{-}\sigma}$ was computed between isopycnals >26.9 and ≤ 27.2 kg m^{-3} (e.g., Figures 9, 10).

ΔT values inside and above the OMZs were compared and discussed for each float separately, because O_2 concentrations differed by 30% between the two sampled regions (e.g., section 1.2.4, and Figures 11, 12). Our main purpose was to assess how the attenuation rates of POC fluxes varied in poorly and well-oxygenated regions relative to the in situ O_2 levels that characterized each sampled region.

Finally, ΔT values were also calculated by using published *absolute* POC fluxes measured by drifting sediment traps and mostly due to large particles in the region sampled by float 6901175 between March and April 2014 (Engel et al., 2017, Figures 9, 10). Thus, ΔT served as normalized metric to independently quantify and compare the remineralized proportion of small and large POC particles in the waters above and inside

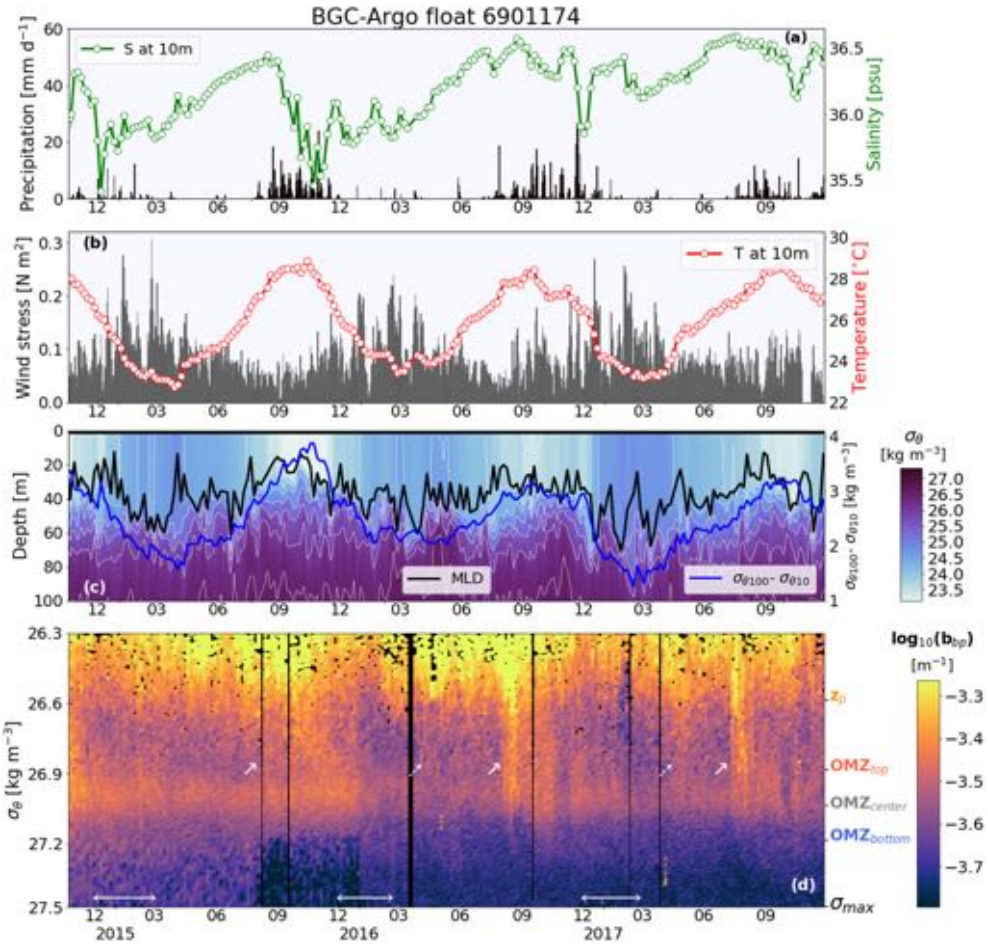

Figure 4. Physical properties and unbiased particle backscattering (b_{bp}) measured by BGC-Argo float 6901174, as well as daily meteorological parameters measured from remote sensing. (a) Mean surface salinity at 10 m depth (green line with white circles) and daily precipitation rates (black bars, data source: https://giovanni.gsfc.nasa.gov/giovanni/). (b) Mean surface temperature at 10 m depth (red line with white circles) and wind stress (gray bars, data source: http://marine.copernicus.eu/). (c) Potential density (σ_Θ) in the first 150 m. The black line refers to the mixed layer depth (MLD) and the blue line is the difference between potential density at 100 m (σ_{100}) and 10 m (σ_{10}) depth. (d) Particle dynamics inferred from b_{bp} measured from isopycnal 26.3 kg m^{-3} to the deepest isopycnal (σ_{max}, near σ_Θ = 27.5 kg m^{-3}) and expressed in logarithmic scale. The locations of productive region (z_p, orange), top (OMZ_{top}, red), center (OMZ_{center}, gray), and bottom (OMZ_{bottom}, blue) of the OMZ, and maximum sampled isopycnal (σ_{max}, black) are indicated in the right y axis. Dashed white and white arrows point to the beginning of the winter-spring and summer-autumn pulses of small particles beneath z_p, respectively. Horizontal white double arrows at the bottom of (d) indicate the periods of no positive net pulses of small particles beneath z_p (e.g., Figures 7, 8).

the OMZ. However, when comparing ΔT values derived from *net* and *absolute* fluxes, it should be kept in mind that these fluxes will differ between them. The reasons of these differences are discussed in section 3.3.

2. Results

2.1. Description of the OMZ and Oxygen Concentrations

The upper, intermediate, and lower water column layers of the OMZ were located between the isopycnals 26.9–27.0, 27.0–27.1, and 27.1–27.2 kg m^{-3}, respectively (Figures 2 and 3). Inside the OMZ, dissolved oxygen concentrations were on average (±standard deviation) 72 μM (±7) and 41 μM (±8) in the regions sampled by floats 6901174 and 6901175, respectively (Figures 2 and 3). Above the OMZ top, O_2 concentrations were 133 μM (±54) and 117 μM (±50) in the regions sampled by floats 6901174 and 6901175, respectively (Figures 2 and 3).

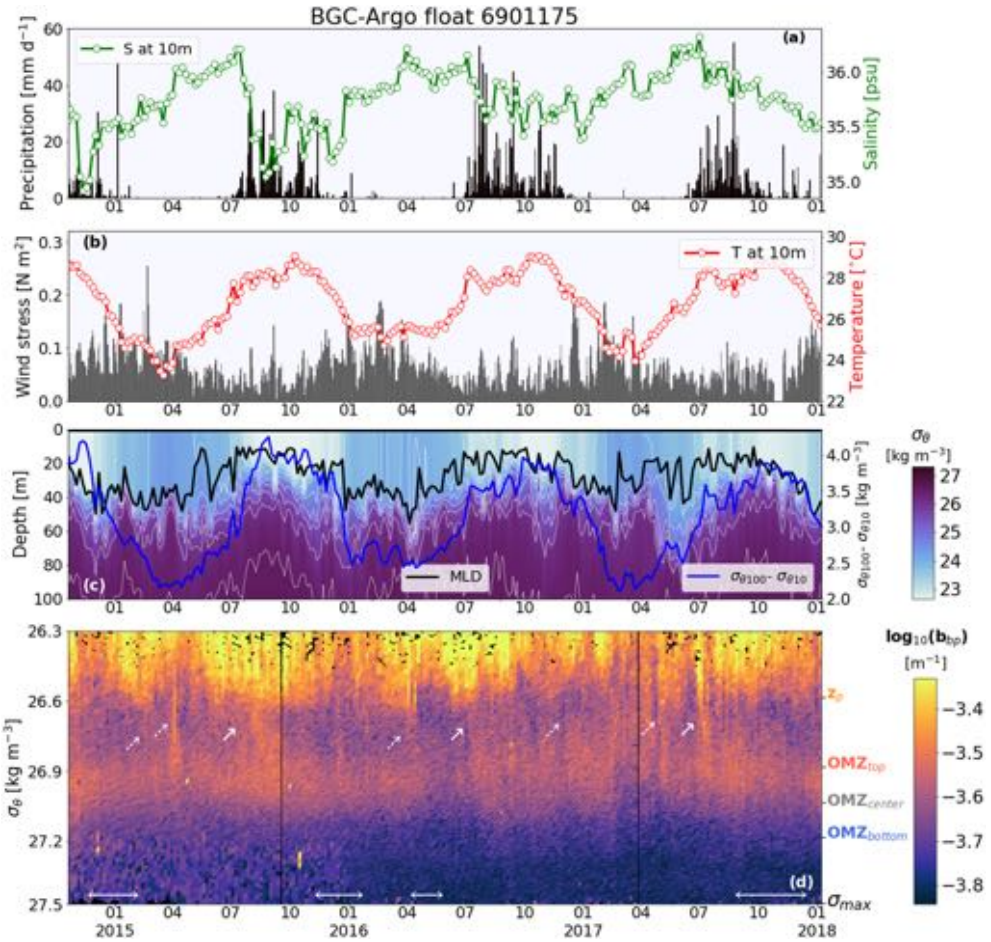

Figure 5. As Figure 4 but for the region sampled by BGC-Argo float 6901175.

2.2. Particle Dynamics and Surface POC Stocks Inferred from b_{bp}

In the ETNA OMZ, maxima and minima of surface stratification were respectively triggered by (1) high precipitation and weak wind stress (June–November) and (2) strong wind stress and no significant precipitation (December–April). These changes in stratification coincided with temporal changes in the dynamics of small particles (0.2–20 μm; Figures 4 and 5). For instance, surface POC stocks reached maximum values when the wind-rain driven surface stratification began between June and September (e.g., Figures 6–8). Weaker increases in surface POC stocks were also observed between the late winter and spring in some of the years, likely due to vertical mixing of nutrients from underlying waters (January–May, period of lower stratification, e.g., Figures 6–8). During this period, surface POC stocks tended to increase only between February and May of 2015 and 2016 in the region sampled by float 6901175 (Figure 8).

A permanent layer relatively rich in small particles was observed in both regions between the upper and intermediate layers of the OMZ (i.e., between isopycnals 26.9–27.1 kg m^{-3}), whereas fewer particles were found below the OMZ_{bottom} ($\sigma_\Theta = 27.2$ kg m^{-3}, Figures 4 and 5). In this permanent layer, mean POC concentrations tended to increase mostly when surface POC stocks accumulated (e.g., Figure 6).

2.3. Surface-Mesopelagic Stocks and Net Instantaneous Fluxes of POC

Surface and mesopelagic POC stocks tended to increase between June–September and January–May (Figures 7, 8). During these periods, large particles could have been exported beneath z_p. Ultimately, the fragmentation of these large particles likely generated pulses of small particles beneath z_p and throughout the mesopelagic (Figures 7, 8). These pulses of small particles beneath z_p are hereafter referred to as summer-autumn and winter-spring pulses, respectively.

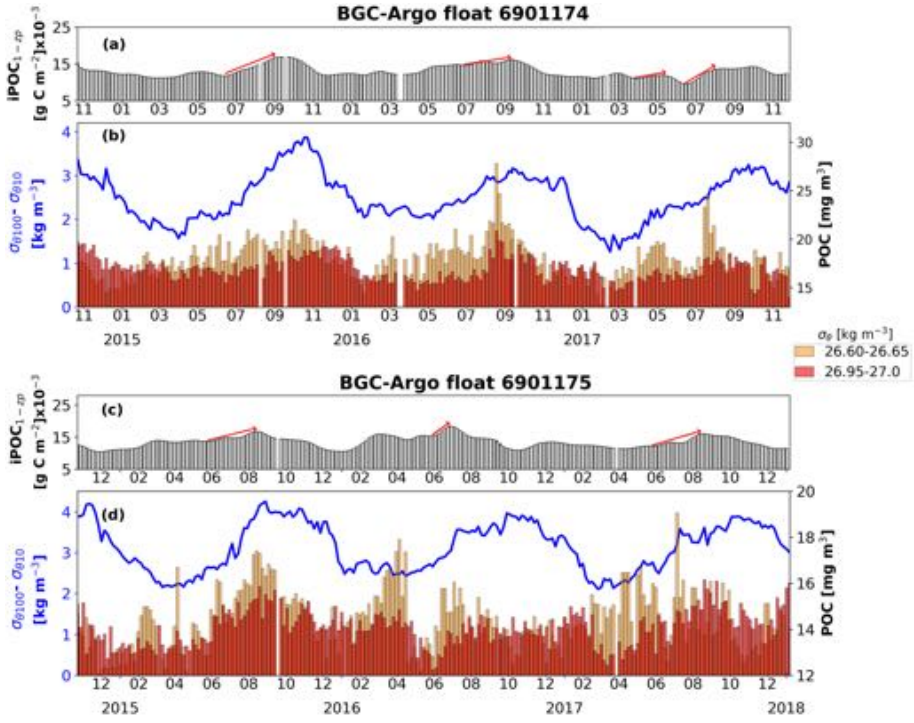

Figure 6. Smoothed surface POC stocks calculated from 1 m to z_p (~130–139 m depth) for floats (a) 6901174 and (c) 6901175. Red lines in (a) and (c) indicate examples of the periods when surface stocks of POC accumulated and generated significant pulses of small particles beneath z_p. (b, d) Temporal changes in mean POC concentrations just between the bottom of the productive region and the top of the OMZ (z_p-OMZ_{top}, 26.60–26.65 kg m^{-3}, yellow bars) and at the upper region of the OMZ (OMZ_{upper}, 26.95–27.0 kg m^{-3}, red bars) for the regions sampled by BGC-Argo floats (b) 6901174 and (d) 6901175. Blue lines in (b) and (d) are the difference between potential density at 100 m (σ_{100}) and 10 m (σ_{10}) depth. This was used as a proxy to unify the temporal effects that external forcings had in surface stratification and related production of surface particles.

When these pulses of small particles occurred, net instantaneous POC fluxes beneath z_p (E_{zp}) ranged between 0.02–12 and 0.1–31 mg C m^{-2} d^{-1} for floats 6901175 and 6901174, respectively (Figures 7 and 8). Nearly simultaneously, maxima of net instantaneous fluxes of POC were also observed within the OMZ (Figures 7 and 8). On the contrary, in the layers below the OMZ_{bottom} ($\sigma_\theta > 27.3$ kg m^{-3}), fluxes tended to be low (e.g., $E_{27.3} = 0.7 \pm 0.7$ mg C m^{-2} d^{-1} for float 6901175, Figure 8).

Flux attenuation rates inside the OMZ were significantly higher than those above the OMZ for 56% of the profiles assessed for float 6901174 ($p < 0.05$, paired t test, number of profiles assessed: 33, Figure 11) and 70% of the profiles assessed for float 6901175 ($p < 0.05$, paired t test, number of profiles assessed: 27, Figure 12).

There were the periods during which small-particle stocks decreased and net instantaneous POC fluxes beneath z_p were negatives (i.e., particles were lost below a given isopycnal). These negatives fluxes ranged between −22.6 and −0.18 mg C m^{-2} d^{-1} for float 69011744 and between −27.3 and −0.03 mg C m^{-2} d^{-1} for float 69011745 (Figures 7 and 8). In addition, there were also specific periods when POC stocks beneath z_p did not change significantly with time (e.g., September–November 2016 for float 6901175, Figure 8).

3. Discussion

3.1. Key Drivers of Net Instantaneous Fluxes of Small Particles

Several forcing mechanisms may contribute to producing and transporting biogenic particles from the sunlit surface toward the ocean interior (e.g., strong summer-export, mixed-layer, eddy-subduction, and local-/large-scale subduction pumps, Boyd et al., 2019; Dall'Olmo et al., 2016; Karl et al., 2012; Omand et al.,

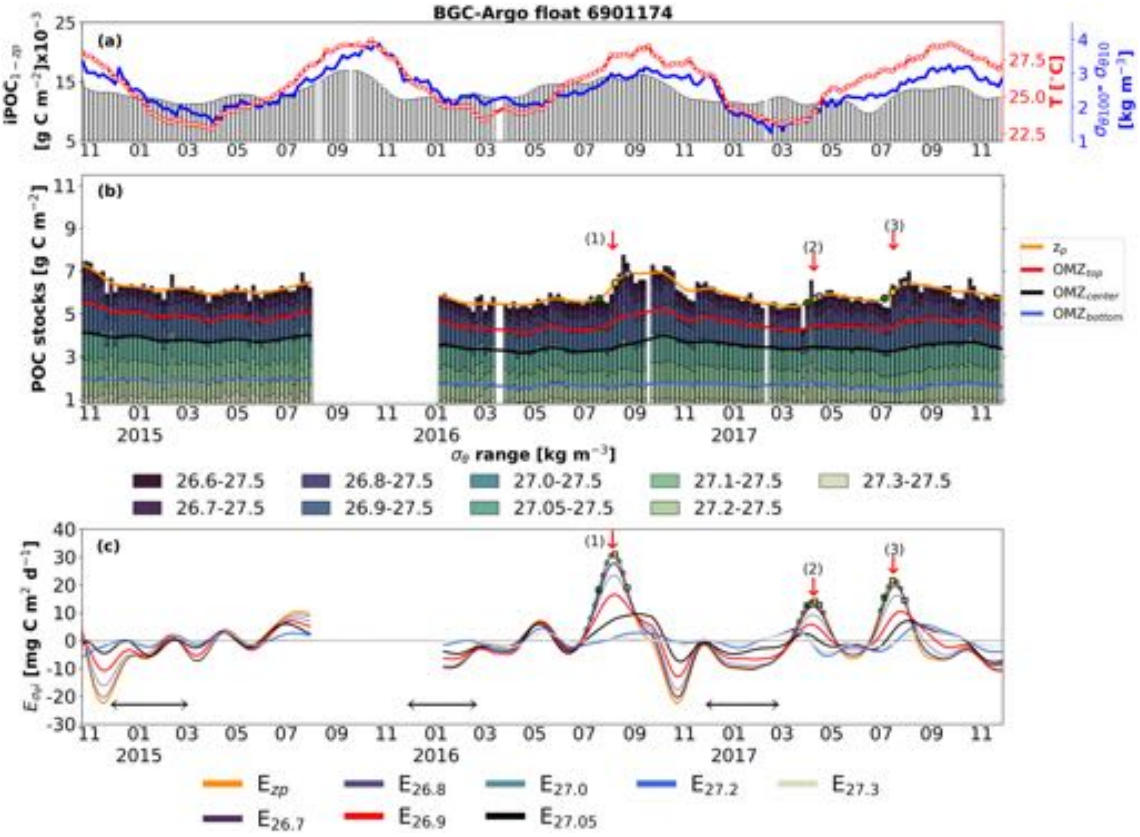

Figure 7. (a) The blue line indicates the difference between potential density at 100 m (σ_{100}) and 10 m (σ_{10}) depth. This was used as a proxy to unify the temporal effects that external forcings had in surface stratification and related production of surface particles. The red line with white circles is the mean surface temperature at 10 m. Gray bars are the smoothed surface stocks of POC calculated from 1 m to z_p (139 ± 12 m). (b) Mesopelagic stocks ($iPOC^{27.5}_{\sigma_{\theta i}}$) and (c) net instantaneous fluxes ($E_{\sigma_{\theta i}}$) of POC for selected layers delimited between z_p ($\sigma_{\theta i}$ = 26.6 kg m^{-3}) and progressively deeper isopynals ($\sigma_{\theta i}$ = 26.65, 26.7, 26.75, ... ,27.45 kg m^{-3}) to σ_{max} ($\sigma_{\theta i}$ = 27.5 kg m^{-3}) for BGC-Argo float 6901174. Orange, red, black, and blue lines in (b) are the smoothed stocks of POC in the productive region (z_p), top (OMZ_{top}), center (OMZ_{center}), and bottom (OMZ_{bottom}) of the OMZ, respectively. White circles and colored squares in (c) are the profiles (n = 27) used to calculate the depth-specific transfer efficiencies (T, % m^{-1}) described in Figures 9–11. Red, yellow, and gray squares are the profiles randomly selected for three temporal events of net instantaneous fluxes of small particles beneath z_p (these temporal events were (1) the summer-autumn pulse of 2016, (2) the winter-spring pulse of 2017, and (3) the summer-autumn pulse of 2017). The latter profiles were used to prepare Figure 11 and those in the supporting information. Black double arrows at the bottom of (c) indicate the periods when there were no positive net pulses of small particles beneath z_p.

2015; Pabortsava et al., 2017). Physical and biological fragmentation of large particles can then generate small particles (Dilling & Alldredge, 2000; Giering et al., 2014; Jumars et al., 1989; Lampitt et al., 1990; Mayor et al., 2014; Stemmann et al., 2004) that can accumulate in the water column, if their removal rates are lower than their production rates.

Here, we hypothesize that two forcing mechanisms might have partially contributed to generate pulses of small particles from z_p to the OMZ: (1) strong summer export events that coincided with higher stratification periods triggered by elevated precipitations and low wind stress (summer-autumn pulses, Figures 7, 8) and (2) local subduction pump linked to wind-driven vertical mixing of nutrients from underlying waters (winter-spring pulses, e.g., Ekman pumping, Boyd et al., 2019; McClain & Firestone, 1993; Pastor et al., 2013; and Figures 7, 8).

Strong summer export events that coincided with stronger stratification appeared to be the most important mechanism related to the net accumulation of small particles inside the productive layer and their export beneath z_p (summer-autumn pulses, Figures 7, 8). This export of POC beneath z_p ranged between 0.02 and 31 mg C m^{-2} d^{-1}. These values are of same order of magnitude of the POC fluxes by small particles reported for the subtropical North Atlantic (0.07–14.9 mg C m^{-2} d^{-1}; Durkin et al., 2015) but are smaller

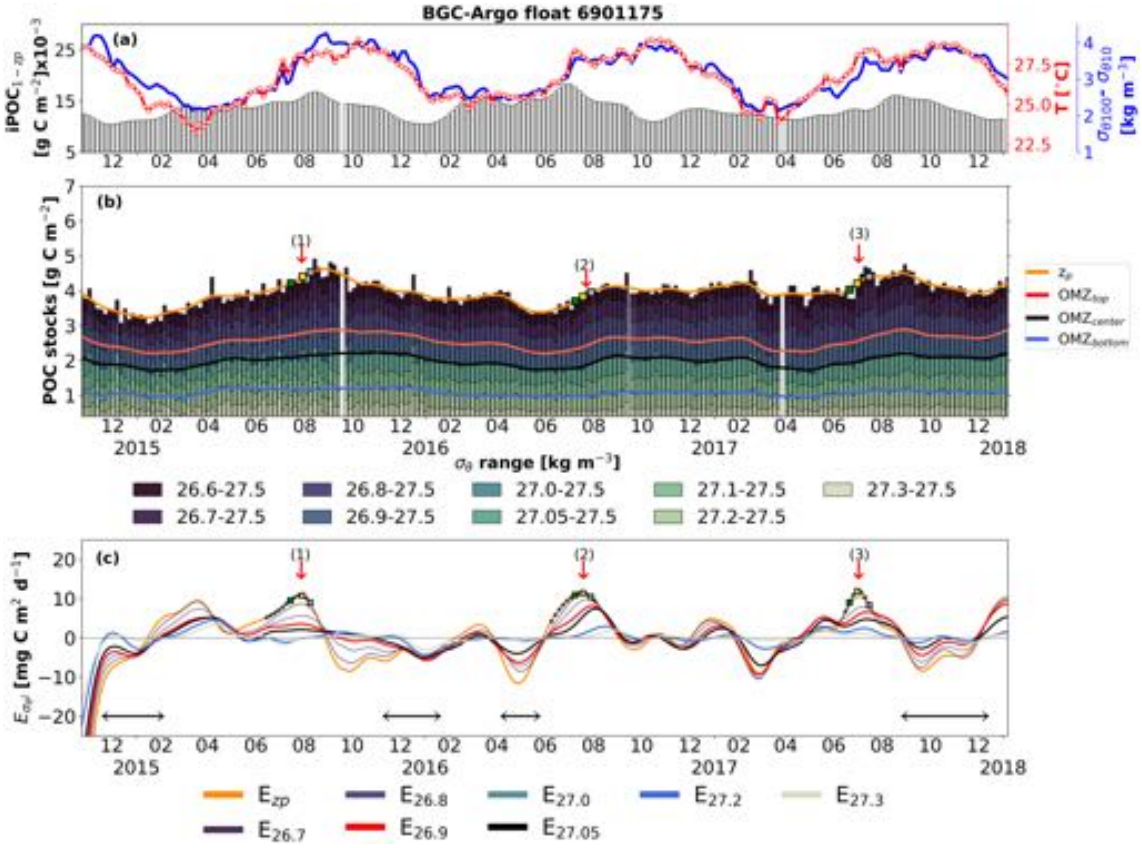

Figure 8. As Figure 7 but for the region sampled by BGC-Argo float 6901175.

than POC fluxes measured in the ETNA by drifting sediment traps and mostly due to large particles (49–61 mg C m^{-2} d^{-1} at 150 m depth, Arístegui et al., 2009; Buesseler et al., 2007; Engel et al., 2017; Gardner et al., 1985; Trull et al., 2008).

Summer-autumn pulses contributed on average around 65% (±16%) to the net annual fluxes of small particles beneath z_p (230 ± 54 mg C m^{-2} $year^{-1}$). These pulses of small particles were likely triggered by a complex synergy of meteorological, physical, and biogeochemical mechanisms. For instance, in this region, Saharan dust and related iron are efficiently scavenged and deposited on the surface ocean by wet deposition (Kieber et al., 2003, 2005; Schlosser et al., 2014; Shi et al., 2012). As a result, the surface ocean becomes enriched in dissolved iron (DFe) and *Trichodesmium* abundance tends to increase by 1–2 orders of magnitude (Schlosser et al., 2014; Snow et al., 2015). Ultimately, *Trichodesmium* blooms collapse and might generate strong episodic exports of large sinking particles possibly reinforced by ballasting effect (Iversen & Robert, 2015; Pabortsava et al., 2017; van der Jagt et al., 2018).

The above hypothesis was partially supported by the progressive accumulation of surface small particles after precipitation events (and inferred related DFe deposition) and subsequent stratification began during the summer in most of the years (e.g., between June and September, Figures 7, 8). Accumulation of small particles likely followed physical and biological fragmentation of large sinking particles generated after phytoplankton blooms collapsed (e.g., *Trichodesmium*). Ultimately, fragmentation might have increased small-particle POC in the mesopelagic region during summer and autumn (Figures 7, 8).

Net annual POC fluxes beneath z_p (E_{zp}) due to winter-spring pulses were on average ~2 times lower than those generated by summer-autumn pulses. In addition, the former E_{zp} values showed a high temporal variability (Figures 7, 8). We hypothesize that this temporal variability in the E_{zp} values was at least in part due to changes in the amount of nutrients injected from underlying waters to z_p (e.g., due to variations in wind-driven vertical mixing of nutrients, McClain & Firestone, 1993; Pastor et al., 2013).

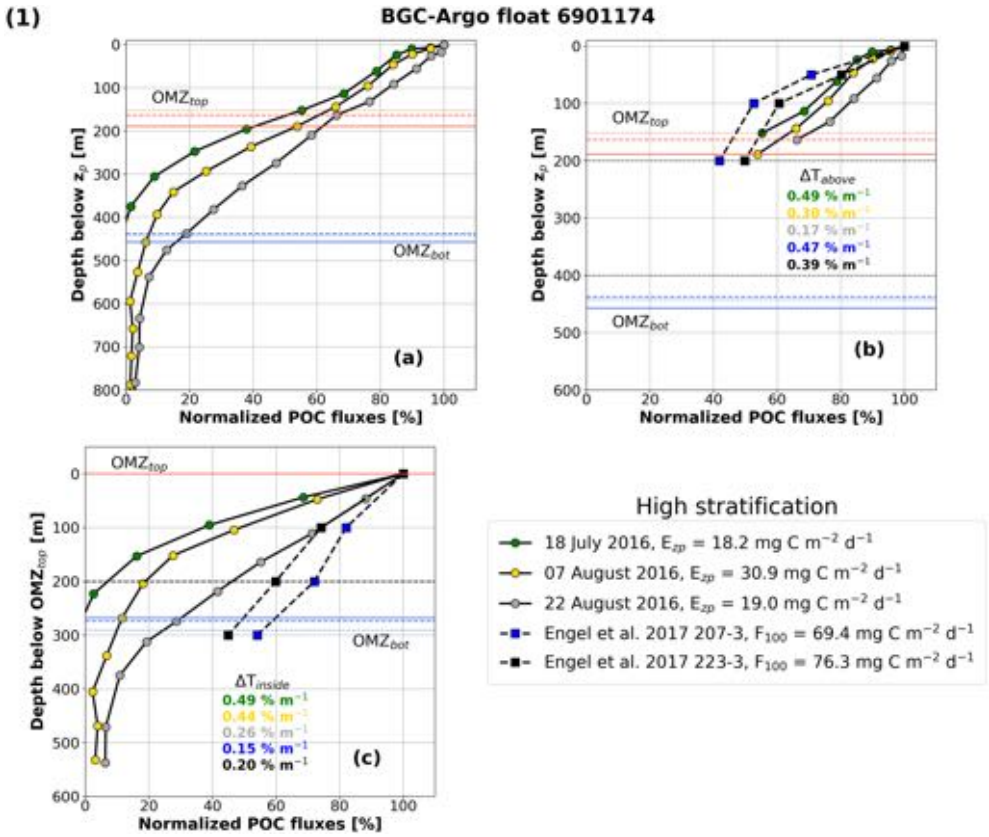

Figure 9. Transfer efficiencies (T_{eff}, %) of net instantaneous POC fluxes ($E_{z\sigma}$) by using the reference depths (a, b) of the productive region (z_p) and (c) top of the OMZ (OMZ_{top}). In (a) we included T_{eff} values for all water column layers beneath z_p while in (b) only those between z_p and top of the OMZ (OMZ_{top}). (c) T_{eff} values of all water column layers beneath OMZ_{top} for BGC-Argo float 6901174. Orange and blue horizontal lines (dashed, dotted, and solid) indicate the top and bottom of the OMZ for selected profiles; whereas horizontal and dotted black lines in (b) and (c) are the locations of the top and bottom of the OMZ defined by Engel et al., 2017, respectively. Green, yellow, and gray circles refer to T_{eff} values of the profiles selected for the summer-autumn pulse of 2016 indicated in Figure 7 (temporal event number 1). Blue and black squares are T_{eff} values calculated from absolute POC fluxes measured by drifting sediment traps in the region sampled by BGC-Argo floats 6901175 between March and April 2014 (Engel et al., 2017, https://doi.pangaea.de/10.1594/PANGAEA.874268). F_{100} and E_{zp} describe POC fluxes at the reference depths defined by Engel et al., 2017 (100 m) and in this study (~130 m), respectively. Depth-specific transfer efficiencies (T, % m^{-1}) were calculated in well- and poorly oxygenated waters layers located between (1) z_p and OMZ_{top} (T_{above}) and (2) OMZ_{top} and bottom of the OMZ (T_{inside}), respectively. Mean T values are described as colored numbers that match with the symbols colors of the profiles selected (circles) and those derived from absolute POC fluxes (squares).

Negative net instantaneous fluxes of POC were observed after the end of the winter-spring and summer-autumn pulses beneath z_p (E_{zp}, Figures 7, 8). The observed temporal variability in these negative fluxes was likely driven by the differences between the rates at which surface small particle was produced and remineralized. For example, the most negative rates of E_{zp} were found between September–December of 2015 and April–May of 2016 for float 69011745 (Figure 8). This probably indicated that the remineralization rates of small particles beneath z_p were more significant than their surface production rates during this period (e.g., between September 2015 and February of 2016, Figure 8). For the same float, the decrease of POC stocks was less steep between September and December of 2016 (E_{zp} ranged between −3.0 and −0.7 mg C m^{-2} d^{-1}, Figure 8). We hypothesize that these differences between the removal and production rates of small particles were low because episodic events of production of surface POC occurred during this period (e.g., October and November of 2016, Figure 8).

In summary, two main mechanisms could have contributed to surface production of small particles and related carbon transfer from z_p toward the OMZ interior: (1) a strong summer export that coincided with higher stratification periods triggered by low wind stress and elevated precipitations (plus inferred related

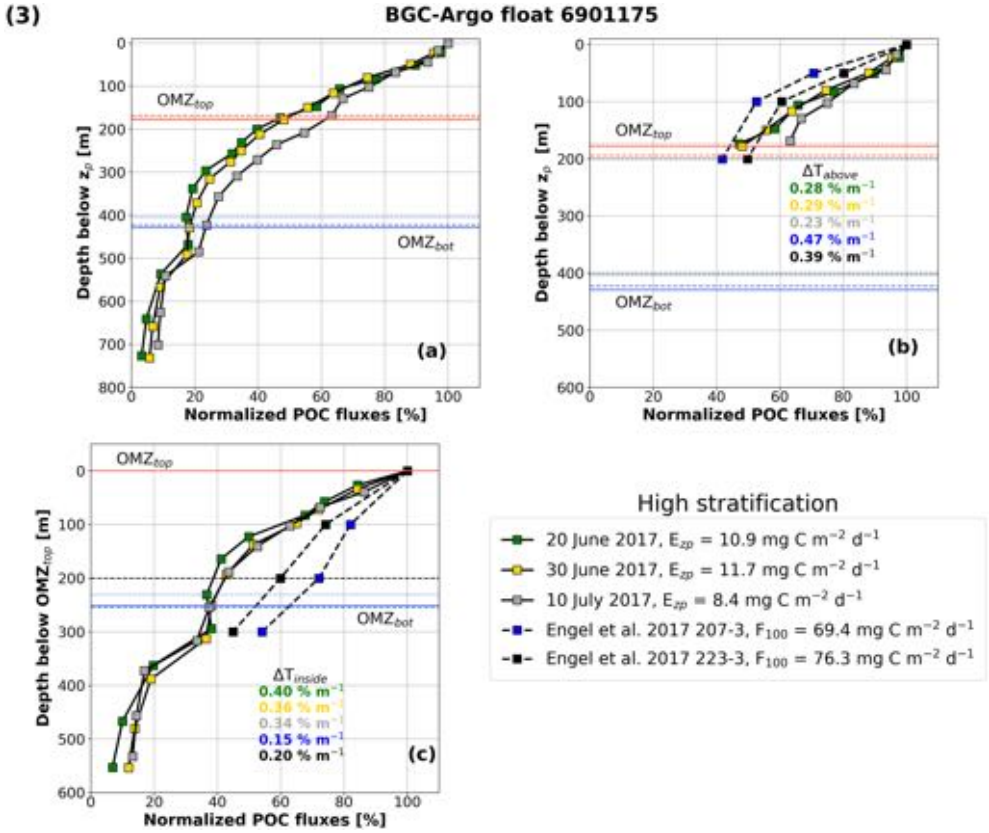

Figure 10. As Figure 9 but for BGC-Argo float 6901175.

DFe deposition, *Trichodesmium* blooms, and their collapse) and (2) the local subduction pump linked to wind-driven vertical mixing of nutrients from underlying waters. However, as we will discuss in next sections, these mechanisms might not be as efficient in exporting small-particle POC (0.2–20 μm) to the ocean interior as previously suggested for large particles in the same region (e.g., Engel et al., 2017).

3.2. Dynamics of the Permanent Layer of Small Particles Inside the OMZ

Anoxic OMZs (O_2 < 5 μM) are characterized by a permanent layer of suspended particles likely related to anaerobic microbial communities (e.g., Günter et al., 2008; Karl & Knauer, 1991; Ulloa et al., 2012; Whitmire et al., 2009; Wojtasiewicz et al., 2018). Here, to the best of our knowledge, we report for the first time that this feature might not be unique to anoxic OMZs because a permanent layer relatively rich in small particles was found between the upper and intermediate layers of the hypoxic OMZ of the ETNA (Figures 4, 5).

Within the OMZ, the concentrations and stocks of POC reached their maxima after the winter-spring and summer-autumn pulses occurred (Figures 6–8). However, the permanent OMZ layer of small particles persisted for the whole time series in both regions (Figures 4, 5). This persistence, even outside of periods with clear particle fluxes from the surface, suggests small particles might be autonomously produced in the upper layers of the OMZ (Figures 2 and 3). This production is likely linked to the activity of free-living aerobic-microbial communities (e.g., chemosynthesis by Archaea, Engel et al., 2017; Herndl et al., 2005; Löscher et al., 2012; Raven, 2009; Reinthaler et al., 2006; Wright et al., 2012).

In support of this hypothesis, there is evidence of an enhancement in the activity of aerobic-anaerobic heterotrophic bacteria associated with large sinking particles in the upper layers of the OMZ. Engel et al. (2017) reported an increment in (1) the ratio between particle hydrolyzable amino acids (PHAA, a chemical marker of aerobic-anaerobic heterotrophic bacterial growth efficiency) and POC in large sinking particles in the center of the OMZ sampled by float 6901175 between March and April 2014 (Engel et al., 2017, e.g., ~400 m, Figure 3) and (2) the contribution of γ-amino butyric acid (a proxy of aerobic-anaerobic heterotrophic bacterial decomposition activity; Lee & Cronin, 1982) to the PHAA in sinking large particles in the top of the

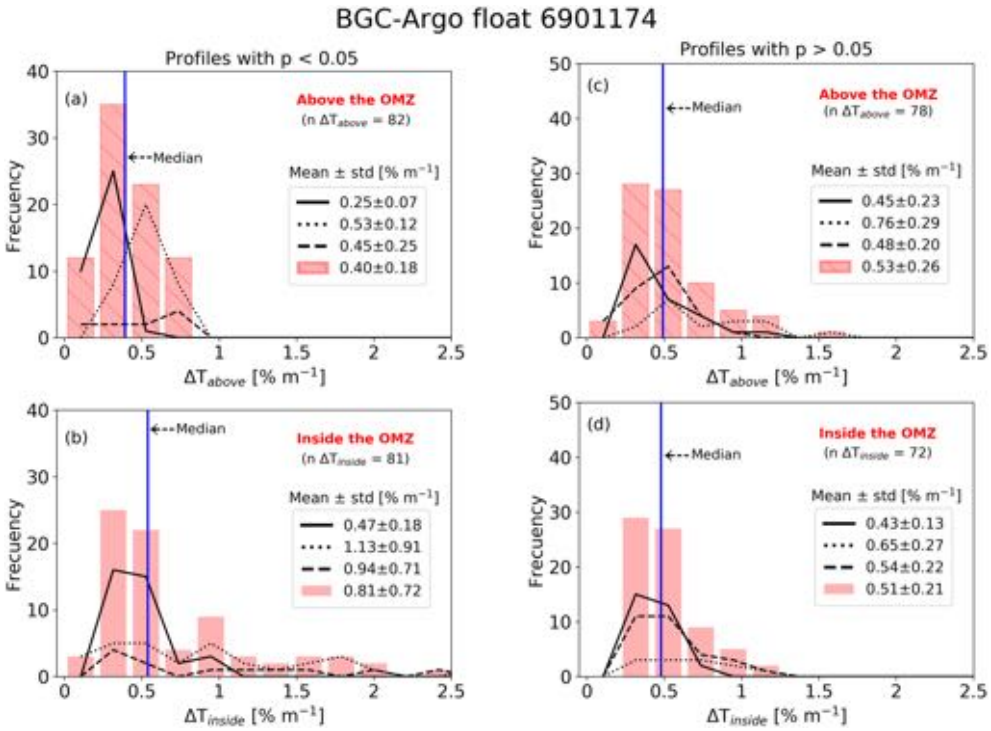

Figure 11. Frequency distributions of depth-specific transfer efficiencies (T, % m^{-1}) calculated above (a, c, red bars with diagonal lines) and inside (b, d, red bars) the OMZ for selected profiles for float 6901174 (see also Figure 7c). Profiles with significant differences between T values inside and above the OMZ are described in the left panel (a and b, n profiles = 14, $p < 0.05$, paired *t* test). Otherwise in the right panel (c and d, n profiles = 13, $p > 0.05$, paired *t* test). Bars summarize T values with (a and b) and without (c and d) significant differences for the profiles of the three temporal events selected (see also Figure 7). Solid, dotted, and dashed black lines only include T values for the profiles of the temporal events 1, 2, and 3, with $p < 0.05$ (a, b), and $p > 0.05$ (c, d), respectively (see also Figure 7). "n T_{inside}" and "n T_{above}" are the total number of T values calculated above and inside the OMZ (red bars). Blue vertical lines indicate the medians of the T values reported for (a) 0.39 % m^{-1}, (b) 0.54 % m^{-1}, (c) 0.49 % m^{-1}, and (d) 0.48 % m^{-1}.

OMZ in the same region and sampled period (Engel et al., 2017, e.g., ~300 m, Figure 3). These two pieces of evidence are consistent with large particles intercepting a large number of free-living aerobic-heterotrophic bacteria in the same part of the water column where we observed the permanent layer of small particles (e.g., Archea, Löscher et al., 2012). However, we cannot rule out that at low oxygen levels (<90 μM), anaerobic-heterotrophic bacteria colonization of the large particles interior could have been induced by the expected expansion of their anoxic core. Ultimately, this could also contribute to increasing the concentration of both chemical markers (PHAA and γ-amino butyric acid, Bianchi et al., 2018; Klawonn et al., 2015).

During the periods without pulses of small particles, we registered negative values of net instantaneous fluxes of POC in just the center of the OMZ (Figures 7, 8). These results suggest that (1) within the permanent layer of particles presumably linked to aerobic-heterotrophic bacteria, net consumption of exported small particles was significant during these periods and (2) this layer was not a net source of small particles to deeper layers (>500 m) of the ETNA. On the contrary, as discussed in the next section, this layer might have acted as a barrier for small particles derived from the fragmentation of large sinking particles.

3.3. Depth-Specific Attenuation Above and Inside the OMZ

The hypothesis that the potential expansion of anoxic and hypoxic OMZs will increase the efficiency with which POC is transported to the ocean's interior appears to be strengthening (e.g., Cavan et al., 2017; Engel et al., 2017; Le Moigne et al., 2017). However, inside the ETNA OMZ, the attenuation rates of net POC fluxes by small particles were significantly higher than those above the OMZ for 62% of the profiles ($p < 0.05$, paired *t* test, Figures 11, 12). For the remaining 38% of the profiles, the attenuation rates of the

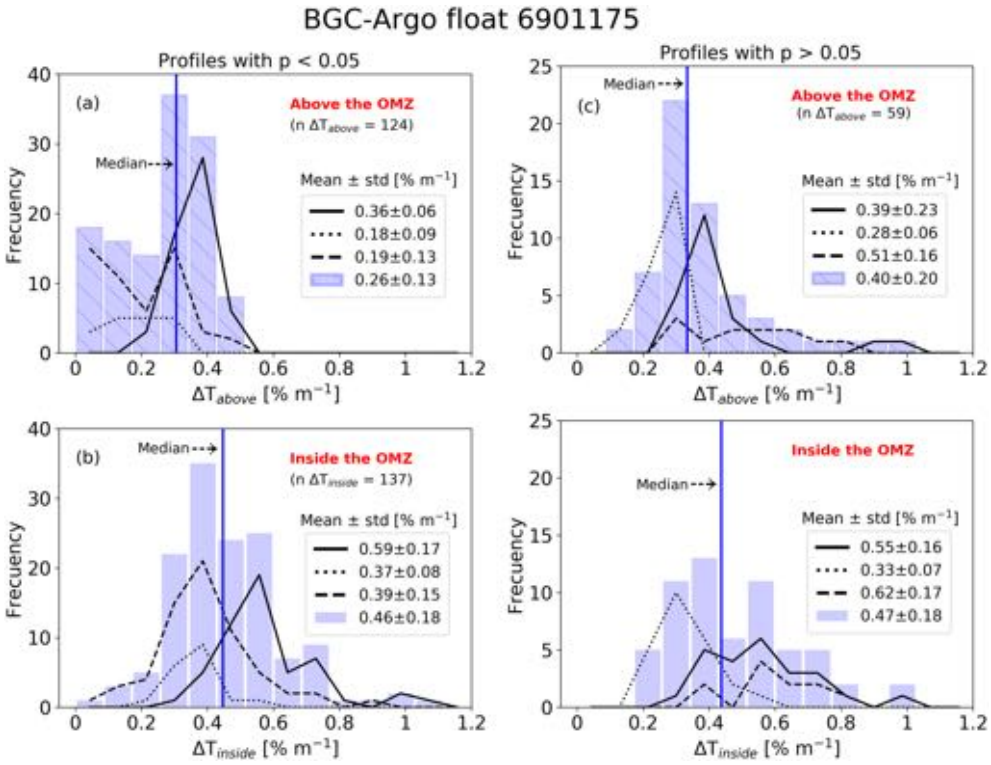

Figure 12. As Figure 11 but for BGC-Argo float 6901175.

fluxes were not significantly different above and inside the hypoxic OMZ ($p > 0.05$, paired *t* test, Figures 11, 12). Thus, our results suggest that the above hypothesis might need to be revised for small-particle fluxes in hypoxic OMZs like the ETNA OMZ.

In addition, inside the ETNA OMZ, flux attenuation tended to decrease with depth (Figures 9, 10). This might indicate that inside this layer (1) small particles derived from the fragmentation of large sinking particles became more recalcitrant with depth and/or (2) flux attenuation was low below the permanent layer of small particles, likely because most of the labile POC is consumed in this layer.

When we compared our estimates to flux attenuations computed from published data (Engel et al., 2017), we found differences that are worth discussing. Specifically, the mean ΔT values estimated above the OMZ were quantitatively similar to those estimated from *absolute* fluxes of POC measured by drifting sediment traps in the same region ($p > 0.05$, *t* test), although these measurements were collected during a different period of the year (March–April 2014; Engel et al., 2017, and Figures 9, 10, 13, and supporting information). In contrast, inside the OMZ, our mean ΔT was significantly higher ($p < 0.05$, *t* test) than that derived for *absolute* fluxes of POC in the study of Engel et al. (2017) (Figures 9, 10, Figure 13). To understand these differences, we need to remember that our ΔT values were derived from *net instantaneous* fluxes of *small* particles instead of *absolute* fluxes of *large* sinking particles.

The *net* instantaneous POC fluxes beneath z_p reported in our study (0.02–31 mg C m^{-2} d^{-1}) were lower than the published *absolute* fluxes at similar depths (49–76 mg C m^{-2} d^{-1}). We propose three main reasons to explain these differences: (1) our *net* fluxes of POC are only measurable when the production of small particles is larger than their loss and thus are a lower bound for the *absolute* fluxes (POC fluxes at the steady state cannot be quantified). (2) Our flux estimates only include the contribution of particles smaller than at most 20 μm (Organelli et al., 2018). Finally, (3) to estimate the rate of change of POC stocks, data were smoothed, which decreased even more the *net* instantaneous fluxes of POC via small particles. These differences must be kept in mind when comparing ΔT values derived from *net* and *absolute* fluxes.

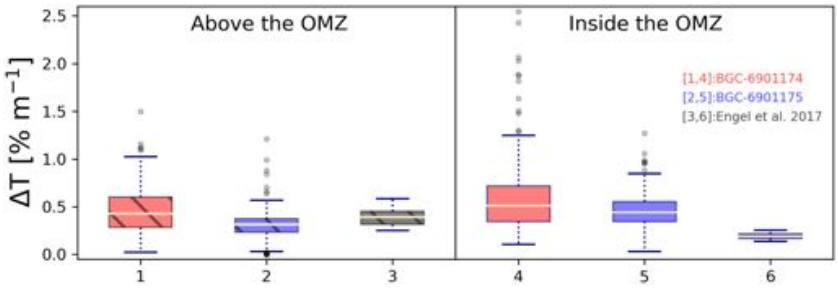

Figure 13. Box plots of depth-specific transfer efficiencies (T, % m^{-1}) above (left panel) and inside (right panel) the OMZ for selected profiles of floats 6901174 (red boxes; see also Figure 7c) and 6901175 (blue boxes; see also Figure 8c), respectively. Black boxes are T values calculated from absolute POC fluxes measured by drifting sediment traps in the region sampled by floats 6901175 between March and April 2014 (Engel et al., 2017. Upper and lower limits of the boxes are the maximum and minimum values, respectively. Boxes describe the interquartile range (IQR), while internal horizontal lines are the medians. The circles are the outliers (3 × IQR).

Despite these differences, our results highlighted that attenuation rates of small particles in poorly oxygenated regions of the OMZ can be equivalent ($p > 0.05$) or significantly higher ($p < 0.05$) than those in well-oxygenated regions (Figures 11, 12). On the other hand, our analysis of the data from Engel et al. (2017) demonstrated that *absolute* POC fluxes of large particles were less attenuated inside the OMZ ($p < 0.05$, *t* test, Figure 13).

We thus expect that inside the OMZ, the contribution of small particles to the total POC fluxes (small + large particles) would be reduced relative to the shallower well-oxygenated regions (e.g., ≤280 m depth). We hypothesize that this is because the permanent layer of small particles, partially linked to heterotrophic bacteria, consumes surface-derived small-particle POC more efficiently than large particles. In addition, it cannot be ruled out that large sinking particles fragmented less in this region.

With the current data, we cannot test the above hypothesis, but if it was proven true, it would have implications for the efficiency of the BCP. This is because the contribution of small particles to the overall POC fluxes is significant in oxygenated regions of the mesopelagic Atlantic at subtropical (41 ± 20%, 11–64 μm, Durkin et al., 2015) and high latitudes (86 ± 23 %, <100 μm, Giering et al., 2016). However, as indicated above, this contribution would be reduced within the hypoxic OMZs. We therefore recommend that more information about POC fluxes by small and large particles and the processes that drive their distribution throughout the water column of the hypoxic OMZs is needed (e.g., remineralization, aggregation/fragmentation rates of large particles). Ultimately, this additional information will allow us to understand how the potential expansion of the hypoxic OMZs will affect the efficiency of the oceans in sequestering atmospheric CO_2.

Finally, a new metric, the depth-specific attenuation (ΔT) rate, was presented based on an extension of the method proposed by Buesseler and Boyd (2009). This metric can provide estimates of POC-flux attenuation rates that are independent of the thickness of the layer over which the fluxes are determined. Thus, it can allow one to compare attenuation rates in different layers of the water column. We exploited this new metric to compare flux attenuation rates above and within the ETNA OMZ.

4. Conclusions

We conclude that (1) the main factor that promoted net instantaneous POC fluxes via small particles toward the OMZ was the strong summer pulse of small particles that coincided with stronger stratification. This stronger stratification was triggered by temporal changes in precipitation (plus inferred related DFe deposition, *Trichodesmium* blooms, and their collapse) and wind stress; (2) similarly to anoxic OMZs, a permanent layer rich in small particles of presumably free-living anaerobic-heterotrophic bacteria was found in the upper part of the hypoxic ETNA OMZ; (3) this permanent layer did not appearto have a measurable net input of POC toward deeper water masses; and (4) inside the hypoxic region of the ETNA, the attenuation rates of net instantaneous small-particle fluxes were equivalent ($p > 0.05$) or significantly higher ($p < 0.05$) than those in well-oxygenated regions. These results differ from those

obtained from absolute POC fluxes measured by drifting sediment traps and mostly due to large particles. These differences highlight the need to better understand the processes controlling the stocks and fluxes of small and large particles in hypoxic OMZs. Progress in this direction will help to better understand the role that hypoxic OMZs have in attenuating POC fluxes. Finally, our results confirm that BGC-Argo floats are powerful tools to fill knowledge gaps related to particle dynamics and their role in the oceanic BCP.

Data Availability Statement

Data from Biogeochemical-Argo floats are freely available at ftp.ifremer.fr/ifremer/argo. These data were collected and made freely available by the International Argo Program and the national programs that contribute to it (http://www.argo.ucsd.edu, The Argo Program is part of the Global Ocean Observing System. Data of wind stress and daily area-averaged precipitation rates applied in this study are also freely available at the websites of the Copernicus Marine Environment Monitoring Service (http://marine.copernicus.eu/services-portfolio/access-to-products/) and Giovanni-NASA (https://giovanni.gsfc.nasa.gov/giovanni/), respectively.

Acknowledgments
The authors would like to thanks to 1) the UK National Academy-the Royal Society, and 2) the European Commission for the support provided to Dr. Rafael Rasse in the framework of the Newton International Fellowship (grant NF150203), and the Marie Skłodowska-Curie Individual Fellowship (grant 839062), respectively. This study is a contribution to the international IMBER project and was supported by (1) the UK Natural Environment Research Council National Capability funding to Plymouth Marine Laboratory and the National Oceanography Centre, Southampton, (2) Horizon 2020 Framework Programme (grant GA 633211), and (3) UK Natural Environment Research Council (grant NE/L012855/1). This is contribution number 337 of the AMT program.

References

Arístegui, J., Gasol, J. M., Duarte, C. M., & Herndld, G. J. (2009). Microbial oceanography of the dark ocean's pelagic realm. *Limnology and Oceanography*, *54*(5), 1501–1529. https://doi.org/10.4319/lo.2009.54.5.1501

Bianchi, D., Weber, T. S., Kiko, R., & Deutsch, C. (2018). Global niche of marine anaerobic metabolisms expanded by particle microenvironments. *Nature Geoscience*, *11*(4), 263–268. https://doi.org/10.1038/s41561-018-0081-0

Bishop, J. K., & Wood, T. J. (2009). Year-round observations of carbon biomass and flux variability in the Southern Ocean. *Global Biogeochemical Cycles*, *23*, GB2019. https://doi.org/10.1029/2008GB003206

Boyd, P. W., Claustre, H., Levy, M., Siegel, D. A., & Weber, T. (2019). Multi-faceted particle pumps drive carbon sequestration in the ocean. *Nature*, *568*(7752), 327–335. https://doi.org/10.1038/s41586-019-1098-2

Briggs, N., Perry, M. J., Cetinić, I., Lee, C., D'Asaro, E., Gray, A. M., & Rehm, E. (2011). High-resolution observations of aggregate flux during a sub-polar North Atlantic spring bloom. *Deep Sea Research Part I: Oceanographic Research Papers*, *58*(10), 1031–1039. https://doi.org/10.1016/j.dsr.2011.07.007

Buesseler, K. O., Antia, A. N., Chen, M., Fowler, S. W., Gardner, W. D., Gustafsson, O., & Steinberg, D. K. (2007). An assessment of the use of sediment traps for estimating upper ocean particle fluxes. *Journal of Marine Research*, *65*(3), 345–416. https://doi.org/10.1357/002224007781567621

Buesseler, K. O., & Boyd, P. W. (2009). Shedding light on processes that control particle export and flux attenuation in the twilight zone of the open ocean. *Limnology and Oceanography*, *54*(4), 1210–1232. https://doi.org/10.4319/lo.2009.54.4.1210

Burd, A. B., & Jackson, G. A. (2009). Particle aggregation. *Annual Review of Marine Science*, *1*, 65–90. https://doi.org/10.1146/annurev.marine.010908.163904

Cavan, E. L., Trimmer, M., Shelley, F., & Sanders, R. (2017). Remineralization of particulate organic carbon in an ocean oxygen minimum zone. *Nature Communications*, *8*, 14847. https://doi.org/10.1038/ncomms14847

Close, H. G., Shah, S. R., Ingalls, A. E., Diefendorf, A. F., Brodie, E. L., Hansman, R. L., et al. (2013). Export of submicron particulate organic matter to mesopelagic depth in an oligotrophic gyre. *Proceedings of the National Academy of Sciences*, *110*(31), 12,565–12,570. https://doi.org/10.1073/pnas.1217514110

Dall'Olmo, G., Dingle, J., Polimene, L., Brewin, R. J., & Claustre, H. (2016). Substantial energy input to the mesopelagic ecosystem from the seasonal mixed-layer pump. *Nature Geoscience*, *9*(11), 820–823. https://doi.org/10.1038/ngeo2818

Dall'Olmo, G., & Mork, K. A. (2014). Carbon export by small particles in the Norwegian Sea. *Geophysical Research Letters*, *41*, 2921–2927. https://doi.org/10.1002/2014GL059244

de Boyer Montégut, C., Madec, G., Fischer, A. S., Lazar, A., & Iudicone, D. (2004). Mixed layer depth over the global ocean: An examination of profile data and a profile-based climatology. *Journal of Geophysical Research*, *109*, C12003. https://doi.org/10.1029/2004JC002378

Deutsch, C., Berelson, W., Thunell, R., Weber, T., Tems, C., McManus, J., et al. (2014). Centennial changes in North Pacific anoxia linked to tropical trade winds. *Science*, *345*(6197), 665–668. https://doi.org/10.1126/science.1252332

Deutsch, C., Brix, H., Ito, T., Frenzel, H., & Thompson, L. (2011). Climate-forced variability of ocean hypoxia. *Science*, *333*(6040), 336–339. https://doi.org/10.1126/science.1202422

Devol, A. H., & Hartnett, H. E. (2001). Role of the oxygen-deficient zone in transfer of organic carbon to the deep ocean. *Limnology and Oceanography*, *46*(7), 1684–1690. https://doi.org/10.4319/lo.2001.46.7.1684

Dilling, L., & Alldredge, A. L. (2000). Fragmentation of marine snow by swimming macrozooplankton: A new process impacting carbon cycling in the sea. *Deep Sea Research Part I: Oceanographic Research Papers*, *47*(7), 1227–1245. https://doi.org/10.1016/S0967-0637(99)00105-3

Durkin, C. A., Estapa, M. L., & Buesseler, K. O. (2015). Observations of carbon export by small sinking particles in the upper mesopelagic. *Marine Chemistry*, *175*, 72–81. https://doi.org/10.1016/j.marchem.2015.02.011

Engel, A., Wagner, H., Le Moigne, F. A., & Wilson, S. T. (2017). Particle export fluxes to the oxygen minimum zone of the eastern tropical North Atlantic. *Biogeosciences*, *14*(7), 1825–1838. https://doi.org/10.5194/bg-14-1825-2017

Estapa, M., Durkin, C., Buesseler, K., Johnson, R., & Feen, M. (2017). Carbon flux from bio-optical profiling floats: Calibrating transmissometers for use as optical sediment traps. *Deep Sea Research Part I: Oceanographic Research Papers*, *120*, 100–111. https://doi.org/10.1016/j.dsr.2016.12.003

Estapa, M. L., Feen, M. L., & Breves, E. (2019). Direct observations of biological carbon export from profiling floats in the subtropical North Atlantic. *Global Biogeochemical Cycles*, *33*, 282–300. https://doi.org/10.1029/2018GB006098

Falkowski, P. G., Barber, R. T., & Smetacek, V. (1998). Biogeochemical controls and feedbacks on ocean primary production. *Science*, *281*(5374), 200–207. https://doi.org/10.1126/science.281.5374.200

Gardner, W. D., Southard, J. B., & Hollister, C. D. (1985). Sedimentation, resuspension and chemistry of particles in the northwest Atlantic. *Marine Geology*, *65*(3-4), 199–242. https://doi.org/10.1016/0025-3227(85)90057-X

Giering, S. L., Sanders, R., Lampitt, R. S., Anderson, T. R., Tamburini, C., Boutrif, M., et al. (2014). Reconciliation of the carbon budget in the ocean's twilight zone. *Nature*, *507*(7493), 480–483. https://doi.org/10.1038/nature13123

Giering, S. L. C., Sanders, R., Martin, A. P., Lindemann, C., Möller, K. O., Daniels, C. J., & St. John, M. A. (2016). High export via small particles before the onset of the North Atlantic spring bloom. *Journal of Geophysical Research: Oceans*, *121*, 6929–6945. https://doi.org/10.1002/2016JC012048

Günter, J., Zubkov, M. V., Yakushev, E., Labrenz, M., & Jürgens, K. (2008). High abundance and dark CO_2 fixation of chemolithoautotrophic prokaryotes in anoxic waters of the Baltic Sea. *Limnology and Oceanography*, *53*(1), 14–22. https://doi.org/10.4319/lo.2008.53.1.0014

Herndl, G. J., Reinthaler, T., Teira, E., van Aken, H., Veth, C., Pernthaler, A., & Pernthaler, J. (2005). Contribution of Archaea to total prokaryotic production in the deep Atlantic Ocean. *Appl. Environ. Microbiol.*, *71*(5), 2303–2309. https://doi.org/10.1128/AEM.71.5.2303-2309.2005

Iversen, M. H., & Robert, M. L. (2015). Ballasting effects of smectite on aggregate formation and export from a natural plankton community. *Marine Chemistry*, *175*, 18–27. https://doi.org/10.1016/j.marchem.2015.04.009

Jumars, P. A., Penry, D. L., Baross, J. A., Perry, M. J., & Frost, B. W. (1989). Closing the microbial loop: Dissolved carbon pathway to heterotrophic bacteria from incomplete ingestion, digestion and absorption in animals. Deep Sea Research Part A. *Oceanographic Research Papers*, *36*(4), 483–495. https://doi.org/10.1016/0198-0149(89)90001-0

Karl, D. M., Church, M. J., Dore, J. E., Letelier, R. M., & Mahaffey, C. (2012). Predictable and efficient carbon sequestration in the North Pacific Ocean supported by symbiotic nitrogen fixation. *Proceedings of the National Academy of Sciences*, *109*(6), 1842–1849. https://doi.org/10.1073/pnas.1120312109

Karl, D. M., & Knauer, G. A. (1991). Microbial production and particle flux in the upper 350 m of the Black Sea. *Deep Sea Research Part A. Oceanographic Research Papers*, *38*, S921–S942. https://doi.org/10.1016/S0198-0149(10)80017-2

Kieber, R. J., Hardison, D. R., Whitehead, R. F., & Willey, J. D. (2003). Photochemical production of Fe (II) in rainwater. *Environmental Science & Technology*, *37*(20), 4610–4616. https://doi.org/10.1021/es030345s

Kieber, R. J., Skrabal, S. A., Smith, B. J., & Willey, J. D. (2005). Organic complexation of Fe (II) and its impact on the redox cycling of iron in rain. *Environmental Science & Technology*, *39*(6), 1576–1583. https://doi.org/10.1021/es040439h

Klawonn, I., Bonaglia, S., Brüchert, V., & Ploug, H. (2015). Aerobic and anaerobic nitrogen transformation processes in N 2-fixing cyanobacterial aggregates. *The ISME journal*, *9*(6), 1456–1466. https://doi.org/10.1038/ismej.2014.232

Kwon, E. Y., Primeau, F., & Sarmiento, J. L. (2009). The impact of remineralization depth on the air-sea carbon balance. *Nature Geoscience*, *2*(9), 630. https://doi.org/10.1038/ngeo612

Lacour, L., Ardyna, M., Stec, K. F., Claustre, H., Prieur, L., Poteau, A., & Iudicone, D. (2017). Unexpected winter phytoplankton blooms in the North Atlantic subpolar gyre. *Nature Geoscience*, *10*(11), 836. https://doi.org/10.1038/ngeo3035

Lampitt, R. S., Noji, T., & Von Bodungen, B. (1990). What happens to zooplankton faecal pellets? Implications for material flux. *Marine Biology*, *104*(1), 15–23. https://doi.org/10.1007/BF01313152

Le Moigne, F. A., Cisternas-Novoa, C., Piontek, J., Maßmig, M., & Engel, A. (2017). On the effect of low oxygen concentrations on bacterial degradation of sinking particles. *Scientific Reports*, *7*(1), 16722. https://doi.org/10.1038/s41598-017-16903-3

Lee, C., & Cronin, C. (1982). The vertical flux of particulate organic nitrogen in the sea: Decomposition of amino acids in the Peru upwelling area and the equatorial Atlantic. *Journal of Marine Research*, *40*(1), 227–251.

Löscher, C. R., Kock, A., Könneke, M., LaRoche, J., Bange, H. W., & Schmitz, R. A. (2012). Production of oceanic nitrous oxide by ammonia-oxidizing archaea. *Biogeosciences*, *9*(7), 2419–2429. https://doi.org/10.5194/bg-9-2419-2012

Lozier, M. S., Dave, A. C., Palter, J. B., Gerber, L. M., & Barber, R. T. (2011). On the relationship between stratification and primary productivity in the North Atlantic. *Geophysical Research Letters*, *38*, L18609. https://doi.org/10.1029/2011GL049414

Martin, J. H., Knauer, G. A., Karl, D. M., & Broenkow, W. W. (1987). VERTEX: Carbon cycling in the northeast Pacific. *Deep Sea Research Part A. Oceanographic Research Papers*, *34*(2), 267–285. https://doi.org/10.1016/0198-0149(87)90086-0

Martiny, A. C., Vrugt, J. A., & Lomas, M. W. (2014). Concentrations and ratios of particulate organic carbon, nitrogen, and phosphorus in the global ocean. *Scientific Data*, *1*. https://doi.org/10.1038/sdata.2014.48

Mayor, D. J., Sanders, R., Giering, S. L., & Anderson, T. R. (2014). Microbial gardening in the ocean's twilight zone: Detritivorous metazoans benefit from fragmenting, rather than ingesting, sinking detritus: Fragmentation of refractory detritus by zooplankton beneath the euphotic zone stimulates the harvestable production of labile and nutritious microbial biomass. *BioEssays*, *36*(12), 1132–1137. https://doi.org/10.1002/bies.201400100

McClain, C. R., & Firestone, J. (1993). An investigation of Ekman upwelling in the North Atlantic. *Journal of Geophysical Research*, *98*(C7), 12327–12339. https://doi.org/10.1029/93JC00868

Mignot, A., Ferrari, R., & Claustre, H. (2018). Floats with bio-optical sensors reveal what processes trigger the North Atlantic bloom. *Nature Communications*, *9*(1), 190. https://doi.org/10.1038/s41467-017-02143-6

Nobre, P., & Shukla, J. (1996). Variations of sea surface temperature, wind stress, and rainfall over the tropical Atlantic and South America. *Journal of Climate*, *9*(10), 2464–2479. https://doi.org/10.1175/1520-0442(1996)009<2464:VOSSTW>2.0.CO;2

Omand, M. M., D'Asaro, E. A., Lee, C. M., Perry, M. J., Briggs, N., Cetinić, I., & Mahadevan, A. (2015). Eddy-driven subduction exports particulate organic carbon from the spring bloom. *Science*, *348*(6231), 222–225. https://doi.org/10.1126/science.1260062

Organelli, E., Dall'Olmo, G., Brewin, R. J., Tarran, G. A., Boss, E., & Bricaud, A. (2018). The open-ocean missing backscattering is in the structural complexity of particles. *Nature Communications*, *9*(1), 1–11. https://doi.org/10.1038/s41467-018-07814-6

Oschlies, A., Koeve, W., Landolfi, A., & Kähler, P. (2019). Loss of fixed nitrogen causes net oxygen gain in a warmer future ocean. *Nature Communications*, *10*(1), 2805. https://doi.org/10.1038/s41467-019-10813-w

Pabortsava, K., Lampitt, R. S., Benson, J., Crowe, C., McLachlan, R., Le Moigne, F. A., & Tilstone, G. H. (2017). Carbon sequestration in the deep Atlantic enhanced by Saharan dust. *Nature Geoscience*, *10*(3), 189. https://doi.org/10.1038/ngeo2899

Parekh, P., Dutkiewicz, S., Follows, M. J., & Ito, T. (2006). Atmospheric carbon dioxide in a less dusty world. *Geophysical Research Letters*, *33*, L03610. https://doi.org/10.1029/2005GL025098

Pastor, M. V., Palter, J. B., Pelegrí, J. L., & Dunne, J. P. (2013). Physical drivers of interannual chlorophyll variability in the eastern subtropical North Atlantic. *Journal of Geophysical Research: Oceans*, *118*, 3871–3886. https://doi.org/10.1002/jgrc.20254

Paulmier, A., & Ruiz-Pino, D. (2009). Oxygen minimum zones (OMZs) in the modern ocean. *Progress in Oceanography*, *80*(3-4), 113–128. https://doi.org/10.1016/j.pocean.2008.08.001

Rasse, R., Dall'Olmo, G., Graff, J., Westberry, T. K., van Dongen-Vogels, V., & Behrenfeld, M. J. (2017). Evaluating optical proxies of particulate organic carbon across the surface Atlantic Ocean. *Frontiers in Marine Science*, *4*, 367. https://doi.org/10.3389/fmars.2017.00367

Raven, J. A. (2009). Contributions of anoxygenic and oxygenic phototrophy and chemolithotrophy to carbon and oxygen fluxes in aquatic environments. *Aquatic Microbial Ecology*, *56*(2-3), 177–192. https://doi.org/10.3354/ame01315

Reinthaler, T., Van Aken, H., Veth, C., Arístegui, J., Robinson, C., Williams, P. J. L. B., et al. (2006). Prokaryotic respiration and production in the meso- and bathypelagic realm of the eastern and western North Atlantic basin. *Limnology and Oceanography*, *51*(3), 1262–1273. https://doi.org/10.4319/lo.2006.51.3.1262

Riley, J. S., Sanders, R., Marsay, C., Le Moigne, F. A., Achterberg, E. P., & Poulton, A. J. (2012). The relative contribution of fast and slow sinking particles to ocean carbon export. *Global Biogeochemical Cycles*, *26*, GB1026. https://doi.org/10.1029/2011GB004085

Roullier, F., Berline, L., Guidi, L., Durrieu De Madron, X., Picheral, M., Sciandra, A., et al. (2014). Particle size distribution and estimated carbon flux across the Arabian Sea oxygen minimum zone. *Biogeosciences*, *11*(16), 4541–4557. https://doi.org/10.5194/bg-11-4541-2014

Sarmiento, J. L., & Gruber, N. (2006). *Ocean biogeochemical dynamics*. Princeton, NJ: Princeton University Press.

Schlosser, C., Klar, J. K., Wake, B. D., Snow, J. T., Honey, D. J., Woodward, E. M. S., & Moore, C. M. (2014). Seasonal ITCZ migration dynamically controls the location of the (sub) tropical Atlantic biogeochemical divide. *Proceedings of the National Academy of Sciences*, *111*(4), 1438–1442. https://doi.org/10.1073/pnas.1318670111

Schmechtig, C., Claustre, H., Poteau, A., & D'Ortenzio, F. (2014). *Bio-Argo quality control manual for the chlorophyll-a concentration*, (pp. 1–13). Argo Data Management. https://doi.org/10.13155/35385

Schmechtig, C., Poteau, A., Claustre, H., D'ortenzio, F., Giorgio Dall'Olmo, G., & Boss E. (2015). Processing BGC-Argo particle backscattering at the DAC level. https://doi.org/10.13155/39459

Schmidtko, S., Stramma, L., & Visbeck, M. (2017). Decline in global oceanic oxygen content during the past five decades. *Nature*, *542*(7641), 335–339. https://doi.org/10.1038/nature21399

Shi, Z., Krom, M. D., Jickells, T. D., Bonneville, S., Carslaw, K. S., Mihalopoulos, N., et al. (2012). Impacts on iron solubility in the mineral dust by processes in the source region and the atmosphere: A review. *Aeolian Research*, *5*, 21–42. https://doi.org/10.1016/j.aeolia.2012.03.001

Signorini, S. R., Murtugudde, R. G., McClain, C. R., Christian, J. R., Picaut, J., & Busalacchi, A. J. (1999). Biological and physical signatures in the tropical and subtropical Atlantic. *Journal of Geophysical Research*, *104*(C8), 18,367–18,382. https://doi.org/10.1029/1999JC900134

Snow, J. T., Schlosser, C., Woodward, E. M. S., Mills, M. M., Achterberg, E. P., Mahaffey, C., & Moore, C. M. (2015). Environmental controls on the biogeography of diazotrophy and Trichodesmium in the Atlantic Ocean. *Global Biogeochemical Cycles*, *29*, 865–884. https://doi.org/10.1002/2015GB005090

Stemmann, L., Jackson, G. A., & Ianson, D. (2004). A vertical model of particle size distributions and fluxes in the midwater column that includes biological and physical processes—Part I: model formulation. *Deep Sea Research Part I: Oceanographic Research Papers*, *51*(7), 865–884. https://doi.org/10.1016/j.dsr.2004.03.001

Stramma, L., Johnson, G. C., Sprintall, J., & Mohrholz, V. (2008). Expanding oxygen-minimum zones in the tropical oceans. *Science*, *320*(5876), 655–658. https://doi.org/10.1126/science.1153847

Stramma, L., Schmidtko, S., Levin, L. A., & Johnson, G. C. (2010). Ocean oxygen minima expansions and their biological impacts. *Deep Sea Research Part I: Oceanographic Research Papers*, *57*(4), 587–595.

Stramski, D., Boss, E., Bogucki, D., & Voss, K. J. (2004). The role of seawater constituents in light backscattering in the ocean. *Progress in Oceanography*, *61*(1), 27–56. https://doi.org/10.1016/j.pocean.2004.07.001

Stramski, D., Reynolds, R. A., Kahru, M., & Mitchell, B. G. (1999). Estimation of particulate organic carbon in the ocean from satellite remote sensing. *Science*, *285*(5425), 239–242. https://doi.org/10.1126/science.285.5425.239

Sullivan, J. M., Twardowski, M. S., Ronald, J., Zaneveld, V., & Moore, C. C. (2013). Measuring optical backscattering in water. In *Light scattering reviews 7* (pp. 189–224). Berlin, Heidelberg: Springer.

Takeshita, Y., Martz, T. R., Johnson, K. S., Plant, J. N., Gilbert, D., Riser, S. C., & Tilbrook, B. (2013). A climatology-based quality control procedure for profiling float oxygen data. *Journal of Geophysical Research: Oceans*, *118*, 5640–5650. https://doi.org/10.1002/jgrc.20399

Thunell, R. C., Varela, R., Llano, M., Collister, J., Karger, F. M., & Bohrer, R. (2000). Organic carbon fluxes, degradation, and accumulation in an anoxic basin: sediment trap results from the Cariaco Basin. *Limnology and Oceanography*, *45*(2), 300–308. https://doi.org/10.4319/lo.2000.45.2.0300

Trull, T. W., Bray, S. G., Buesseler, K. O., Lamborg, C. H., Manganini, S., Moy, C., & Valdes, J. (2008). In situ measurement of mesopelagic particle sinking rates and the control of carbon transfer to the ocean interior during the Vertical Flux in the Global Ocean (VERTIGO) voyages in the North Pacific. *Deep Sea Research Part II: Topical Studies in Oceanography*, *55*(14-15), 1684–1695. https://doi.org/10.1016/j.dsr2.2008.04.021

Ulloa, O., Canfield, D. E., DeLong, E. F., Letelier, R. M., & Stewart, F. J. (2012). Microbial oceanography of anoxic oxygen minimum zones. *Proceedings of the National Academy of Sciences*, *109*(40), 15,996–16,003. https://doi.org/10.1073/pnas.1205009109

van der Jagt, H., Friese, C., Stuut, J. B. W., Fischer, G., & Iversen, M. H. (2018). The ballasting effect of Saharan dust deposition on aggregate dynamics and carbon export: Aggregation, settling, and scavenging potential of marine snow. *Limnology and Oceanography*, *63*(3), 1386–1394. https://doi.org/10.1002/lno.10779

Van Mooy, B. A., Keil, R. G., & Devol, A. H. (2002). Impact of suboxia on sinking particulate organic carbon: Enhanced carbon flux and preferential degradation of amino acids via denitrification. *Geochimica et Cosmochimica Acta*, *66*(3), 457–465. https://doi.org/10.1016/S0016-7037(01)00787-6

Volk, T., & Hoffert, M. I. (1985). Ocean carbon pumps: Analysis of relative strengths and efficiencies in ocean-driven atmospheric CO2 changes. *The carbon cycle and atmospheric CO2: natural variations Archean to present*, *32*, 99–110. https://doi.org/10.1029/GM032p0099

Whitmire, A. L., Letelier, R. M., Villagrán, V., & Ulloa, O. (2009). Autonomous observations of in vivo fluorescence and particle backscattering in an oceanic oxygen minimum zone. *Optics Express*, *17*(24), 21,992–22,004. https://doi.org/10.1364/OE.17.021992

Wojtasiewicz, B., Trull, T. W., Bhaskar, T. U., Gauns, M., Prakash, S., Ravichandran, M., & Hardman-Mountford, N. J. (2018). Autonomous profiling float observations reveal the dynamics of deep biomass distributions in the denitrifying oxygen minimum zone of the Arabian Sea. *Journal of Marine Systems*. https://doi.org/10.1016/j.jmarsys.2018.07.002

Wojtasiewicz, B., Walsh, I. D., Antoine, D., Slawinski, D., & Hardman-Mountford, N. J. (2018). Inferring and removing a spurious response in the optical backscattering signal from an autonomous profiling float. *Journal of Atmospheric and Oceanic Technology*, *35*(11), 2137–2146. https://doi.org/10.1175/JTECH-D-18-0027.1

Wright, J. J., Konwar, K. M., & Hallam, S. J. (2012). Microbial ecology of expanding oxygen minimum zones. *Nature Reviews Microbiology*, *10*(6), 381–394. https://doi.org/10.1038/nrmicro2778

References From the Supporting Information

Bittig, H. C., Körtzinger, A., Neill, C., van Ooijen, E., Plant, J. N., Hahn, J., et al. (2018). Oxygen optode sensors: Principle, characterization, calibration, and application in the ocean. *Frontiers in Marine Science*, *4*, 429. https://doi.org/10.3389/fmars.2017.00429

Körtzinger, A., Schimanski, J., & Send, U. (2005). High quality oxygen measurements from profiling floats: A promising new technique. *Journal of Atmospheric and Oceanic Technology*, *22*(3), 302–308. https://doi.org/10.1175/JTECH1701.1

Tengberg, A., Hovdenes, J., Andersson, H. J., Brocandel, O., Diaz, R., Hebert, D., et al. (2006). Evaluation of a lifetime-based optode to measure oxygen in aquatic systems. *Limnology and Oceanography: Methods*, *4*(2), 7–17. https://doi.org/10.4319/lom.2006.4.7